NASA Technical Paper 3508

An Inelastic Analysis of a Welded Aluminum Joint

R.E. Vaughan
Marshall Space Flight Center • MSFC, Alabama

National Aeronautics and Space Administration
Marshall Space Flight Center • MSFC, Alabama 35812

September 1994

TABLE OF CONTENTS

LIST OF ILLUSTRATIONS

LIST OF ILLUSTRATIONS (Continued)

LIST OF TABLES

TECHNICAL PAPER

AN INELASTIC ANALYSIS OF A WELDED ALUMINUM JOINT

I. INTRODUCTION

Butt-weld joints are common design features of pressure vessels, and are as reliable as the weakest element in the weld chain. In practice, weld material properties are determined from a tensile test specimen and are provided to the stress analyst in the form of a stress versus strain diagram (fig. 1).

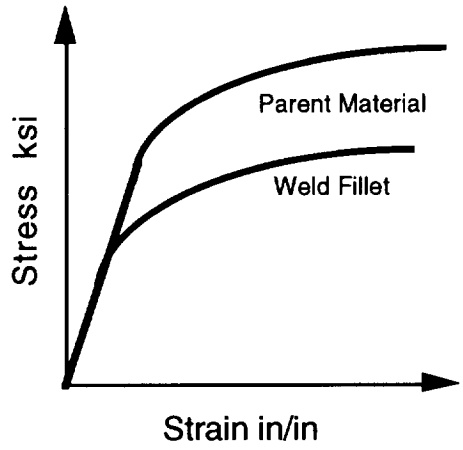

Figure 1. Typical stress-strain curve for welds.

The most common method of analysis assumes the weld is free from residual stresses produced by the welding process and ignores any variation of material properties within the weld. Experimental and analytical investigations of residual stresses and heat-affected zones (HAZ's) are numerous. Rybicki and Stonesifer[1] developed computational models to calculate the magnitude and distribution of residual stresses for multipass welds. Papzoglou and Masubuchi included phase-transformation effects and thermo-elastic-plastic analysis to develop computational methods of determining residual stresses in welds.[2] Agapakis et al.[3] investigated analytical models for the calculation of residual-stress relaxation during stress-relief heat treatments. The softening of material properties in HAZ's has also been studied in great detail. Robertson and Dwight[4] used classical heat-flow theory to determine the extent of HAZ's for multipass welds.

To date, there has been little effort to study the effects of residual stresses and material property variations for loaded weld joints. Postwelding heat treatments, stress-relief techniques, and thermal controls during the welding process are designed to eliminate the detrimental effects of these process-induced variables. However, experimental studies have shown that these variables may be present in a weld even after efforts have been made to remove them.[5-7]

A good welded joint will usually develop the full strength of the material being joined unless the high temperature necessary for the process changes the properties of the materials. The welding process

for thick welds requires high temperatures and, therefore, should be suspect for variations in material properties at the weld. The effects of variations in properties through the thickness of the weld and along the width of the weld are difficult to assess because of the inaccessibility of welds in service applications and because of the costs associated with such studies.

A butt weld is a weld in which two members are joined by machining a groove for the weld material and then butting the remaining parent material together at the ends (fig. 2). Depending on the thickness of the material, it is common to require multiple weld passes to fill the groove. In such a weld, the passes start at midthickness and alternate from one side to another in an effort to provide symmetrical material properties throughout the thickness (fig. 2). In addition to variance through the thickness of the weld, the material properties can vary across the width of the weld due to the presence of an HAZ between the weld material and the parent material. Such welds are currently used in a variety of large aerospace structures. Tests of such structures have often resulted in failures of the weld at measured strain values well below those predicted by currently available computational methods (see e.g., reference 8).

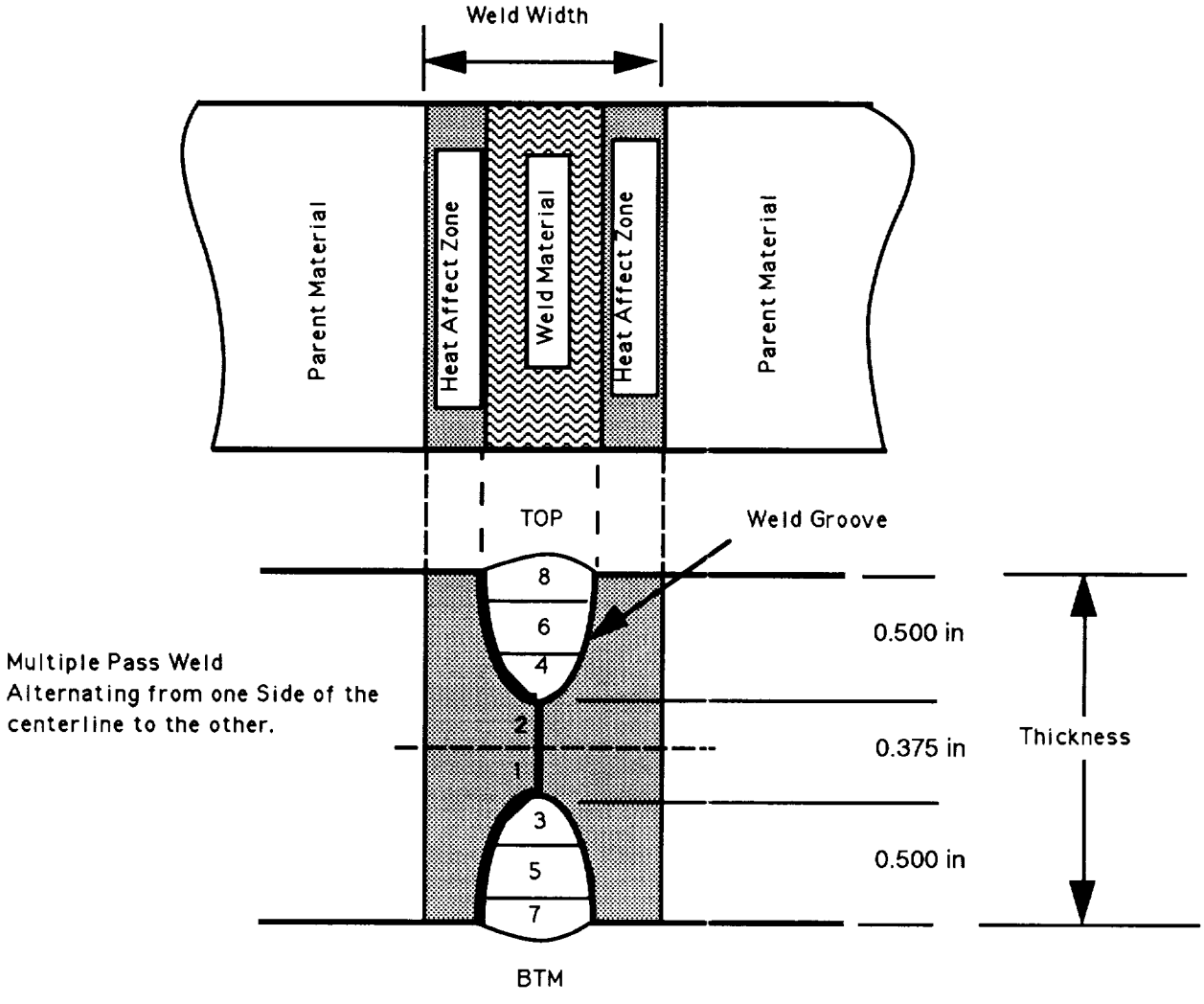

Figure 2. Multiple-pass weld.

In 1991, a NASA-sponsored experimental research project indicated that 2219-T87 aluminum welds exhibit distinct zones of varying material properties across the HAZ and through the thickness of the weld.[4-7] The project initially involved axially loading 2219-T87 specimens with a welded joint in the center. The tests indicated the weld and the HAZ are much more ductile than the parent material.[5] At higher strain values, large amounts of necking is apparent in the weld and HAZ, indicating a complex state of strain in the specimen. Additional investigations using specimens with 1.4-in thickness discovered nonlinear, nonuniform material properties through the weld thickness. One side of the weld specimen was found to be much weaker and more ductile than the other side.[6] Numerical analysis of these test specimens failed to produce predictions consistent with experimental results. The material modeling and the finite-element code were considered inadequate to simulate the true behavior of the weld joint.[4]

The purpose of this study is to investigate analytical and computational methods used for the analysis of a thick weld and to develop an analytical model that can be used to predict the weld response to statically applied loads. The results of the analysis will be compared to experimental data to determine the weld behavior and the accuracy of the analysis methods. The weld considered in this study is a multiple-pass aluminum 2219-T87 butt weld as shown in figure 2. Elasticity and plasticity theory are examined to provide insight into modeling the inelastic properties beyond the weld material elastic limit. A one-dimensional (1–D), single-zone material model is developed to demonstrate the accuracy of the computational method when compared to analytical predictions and to experimental results. The material modeling methods verified in the single-zone material model are then applied to a multiple-zone material model of the same tensile test specimen.

The weld specimen is modeled using the finite-element code *ABAQUS*. The analysis procedure will begin with a linear analysis of the test specimen. The predictions of the finite-element model will be verified by comparison to theory and to test in the elastic region. The material constants for the inelastic analysis will be determined from available test data (stress-strain curve). An analytical model of the test specimen will be developed to verify the inelastic material modeling methods used in the finite-element model. The predictions of the analytical model and the finite-element model will then be compared to the inelastic test data to verify both models. The single-zone material model will provide a benchmark for developing the multiple-zone material model. The material modeling methods verified in the single-zone material model are repeated for each set of material properties used in the multiple-zone material model. The results of the multiple-zone finite-element model analysis will then be compared to test data. As part of the analysis performed in this study, the finite-element model and tensile test data are both used to determine Poisson's ratio in the inelastic region. The computational value is then compared to the value obtained from test data. The results of the comparisons are used to discuss several aspects of multipass weld behavior and to make recommendations concerning future analysis and testing of welds.

Section I contains a development of the equations to be used for the stress and strain calculations to follow. Linear elastic stress-strain equations are presented and compared against inelastic equations. Section II provides an analysis of a welded tensile test specimen using incremental strain theory. Section III develops the computational model of the tensile test specimen. The first computational model assumes the weld has continuous (single-zone) material properties through the thickness of the specimen. In section IV, the second computational model assumes the weld has varying (multiple-zone) material properties through the thickness. In addition, section IV provides a comparison of the computational predictions and the experimental data. Finally, section V offers conclusions and recommendations for future analyses of thick welds.

II. EQUATIONS OF STRESS AND STRAIN

A. Linear Elastic Solutions

Linear elastic solutions are the basis for most structural analyses performed in engineering applications. Concepts from linear elastic theory are presented herein to define terms and to identify and understand similarities between elastic and inelastic methods of analysis.

Consider the three-dimensional normal and shear stress acting on a solid volume as illustrated in figure 3.

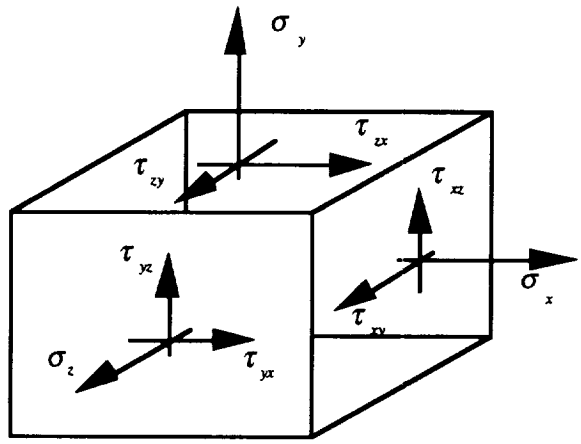

Figure 3. Normal and shear stress orientations.

Engineering stress is defined as the ratio of applied load to the initial cross-sectional area; engineering strain is defined as the ratio of the deflection in the direction of an applied normal load to an original length. The stress-strain diagram of a polycrystalline material in uniaxial tension is illustrated in figure 4.

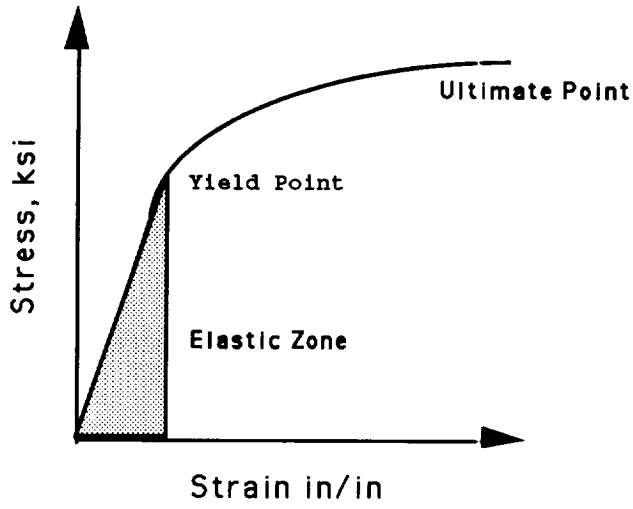

Figure 4. Normal stress-normal strain curve.

The initial linear portion of the stress-strain diagram is the linear elastic region in which the stress is directly proportional to the strain. This relationship is known as Hooke's law. The ratio of stress to strain in a uniaxial specimen is known as the modulus of elasticity or Young's modulus. The application of a load in a uniaxial direction also causes a contraction in the transverse direction for all homogenous, isotropic materials. The absolute value of the ratio of the lateral strain and the axial strain is Poisson's ratio.

Shear strains are produced in a material by the action of shearing stresses. The shear stress-shear strain diagram is similar to the normal uniaxial relationship in figure 4, having a linear and nonlinear region. In the linear region the shear stress and shear strain are also proportional; the constant of proportionality is called the shear modulus. The shear modulus is related to the modulus of elasticity as:

$$G = \frac{E}{2(1+\nu)} \ , \tag{1}$$

where E is Young's modulus, ν is Poisson's ratio, and G is the shear modulus.

The three-dimensional stress-strain relationships derived from the superposition of 1–D Hooke's laws and Poisson's ratio effects are written as follows:

$$\varepsilon_x = \frac{1}{E}\left[\sigma_x - \nu(\sigma_y + \sigma_z)\right] \ , \tag{2a}$$

$$\varepsilon_y = \frac{1}{E}\left[\sigma_y - \nu(\sigma_x + \sigma_z)\right] \ , \tag{2b}$$

$$\varepsilon_z = \frac{1}{E}\left[\sigma_z - \nu(\sigma_x + \sigma_y)\right] \ , \tag{2c}$$

$$\gamma_{xy} = G\tau_{xy} \ , \tag{2d}$$

$$\gamma_{yz} = G\tau_{yz} \ , \tag{2e}$$

$$\gamma_{xz} = G\tau_{xz} \ . \tag{2f}$$

If only normal stresses are applied to a three-dimensional element, a change in the element volume will result. This volume change can be written in terms of the normal strains as:

$$\frac{\Delta V}{V} = \varepsilon_x + \varepsilon_y + \varepsilon_z \ . \tag{3}$$

From equations (2a) through (2f) and (3), the sum of the three normal elastic strains is proportional to the sum of the three normal stress components and is given by:

$$\varepsilon_x + \varepsilon_y + \varepsilon_z = \frac{1-2\nu}{E}\left(\sigma_x + \sigma_y + \sigma_z\right) \ . \tag{4}$$

B. Inelastic Solutions

The stress-strain equations for the inelastic analysis to be performed are similar to the linear elastic equations discussed in the previous section. The derivation of the equations to be used can be found in any one of numerous text books addressing the field of incremental strain theory. The equations presented here can be found in reference 9. Following the procedure in reference 9, the incremental strain equations for the plastic (inelastic) stress-strain region may be written as:

$$d\varepsilon_x^p = \frac{F(\tau_o)}{3\tau_o}\left[\sigma_x - \frac{1}{2}(\sigma_y+\sigma_z)\right]d\tau_o \quad , \tag{5a}$$

$$d\varepsilon_y^p = \frac{F(\tau_o)}{3\tau_o}\left[\sigma_y - \frac{1}{2}(\sigma_x+\sigma_z)\right]d\tau_o \quad , \tag{5b}$$

$$d\varepsilon_z^p = \frac{F(\tau_o)}{3\tau_o}\left[\sigma_z - \frac{1}{2}(\sigma_x+\sigma_y)\right]d\tau_o \quad , \tag{5c}$$

$$d\gamma_{xy}^p = \frac{F(\tau_o)}{\tau_o}\tau_{xy}d\tau_o \quad , \tag{5d}$$

$$d\gamma_{yz}^p = \frac{F(\tau_o)}{\tau_o}\tau_{yz}d\tau_o \quad , \tag{5e}$$

$$d\gamma_{zx}^p = \frac{F(\tau_o)}{\tau_o}\tau_{zx}d\tau_o \quad , \tag{5f}$$

where $F(\tau_o)$ is a function of τ_o, the octahedral shear stress. The octahedral shearing stress can be expressed as follows in terms of the normal and shear stress :

$$\tau_o = \frac{1}{3}\sqrt{(\sigma_x-\sigma_y)^2+(\sigma_y-\sigma_z)^2+(\sigma_z-\sigma_x)^2+6(\tau_{xy}^2+\tau_{yz}^2+\tau_{zx}^2)} \quad . \tag{6}$$

These stress-strain relations are for loading only and differ from equations (5a) through (5f), the linear stress-strain relations, in the following manner:

1. The engineering strain $\varepsilon_x,\varepsilon_y,\varepsilon_z$ and $\gamma_{xy},\gamma_{xz},\gamma_{zy}$ have been replaced by incremental strains $d\varepsilon_x^p,d\varepsilon_y^p,d\varepsilon_z^p$ and $d\gamma_{xy}^p,d\gamma_{xz}^p,d\gamma_{yz}^p$;

2. Young's Modulus has been replaced by $\frac{3\tau_o}{F(\tau_o)}d\tau_o$; and,

3. Poisson's ratio, ν, has been set equal to $1/2$ for all materials.

Bridgman's experiments[10] substantiated the claim that the change in unit volume due to the increments of plastic strain must be zero. The resulting plastic Poisson's ratio can be computed by

considering the sum of the incremental strains in terms of an unknown plastic Poisson's ratio as follows: By adding equations (5a) through (5c) we have

$$d\varepsilon_x^p + d\varepsilon_y^p + d\varepsilon_z^p = \frac{F(\tau_o)}{3\tau_o}\left[\sigma_x - \nu_{pl}(\sigma_y+\sigma_z) + \sigma_y - \nu_{pl}(\sigma_x+\sigma_z) + \sigma_z - \nu_{pl}(\sigma_y+\sigma_x)\right]d\tau_o \ ,$$

which can be rewritten as

$$d\varepsilon_x^p + d\varepsilon_y^p + d\varepsilon_z^p = \frac{F(\tau_o)}{3\tau_o}(1-2\nu_{pl})(\sigma_x+\sigma_y+\sigma_z)d\tau_o \ . \tag{7}$$

Since the left-hand side of the equation must equal zero, it must follow that $\nu_{pl} = 1/2$. This relationship is referred to as the constant-volume assumption.

In order to apply the plastic stress-strain equations, the function $F(\tau_o)$ must be developed. The function $F(\tau_o)$ is a material property and, like most structural material properties, can be derived from a simple tensile test in which $\sigma_y = \sigma_z = 0$, and loads are applied only in the σ_x direction. In such a case, the octahedral shear stress can be written as:

$$\tau_o = \frac{1}{3}\sqrt{(\sigma_x)^2+(\sigma_x)^2} = \frac{\sqrt{2}}{3}\sigma_x \ , \tag{8a}$$

from which it follows that

$$d\tau_o = \frac{\sqrt{2}}{3}d\sigma_x \ . \tag{8b}$$

Now, consider the plastic stress-strain equation for $d\varepsilon_x^p$, given by equation (5a). For the uniaxial tensile test, the following values are substituted into this equation: $\tau_o = \frac{\sqrt{2}}{3}\sigma_x$, $d\tau_o = \frac{\sqrt{2}}{3}d\sigma_x$, $\sigma_y = \sigma_z = 0$. The result is as follows:

$$d\varepsilon_x^p = \frac{F\left(\frac{\sqrt{2}}{3}\sigma_x\right)}{3\left(\frac{\sqrt{2}}{3}\sigma_x\right)}(\sigma_x)\,d\left(\frac{\sqrt{2}}{3}\sigma_x\right) = \frac{1}{3}F\left(\frac{\sqrt{2}}{3}\sigma_x\right)d\sigma_x \ . \tag{9}$$

It is shown in reference 9 that a simple tension test can be used to define a function $f\left(\frac{\sqrt{2}}{3}\sigma_x\right)$ which is related to $d\varepsilon_x^p$ through the following equation:

$$f\left(\frac{\sqrt{2}}{3}\sigma_x\right) = \sqrt{2}\varepsilon_x^p \ . \tag{10a}$$

Taking the derivative of both sides of equation (10a) yields the following equation for incremental plastic strain $d\varepsilon_x^p$:

$$d\varepsilon_x^p = \frac{1}{3} f'\left(\frac{\sqrt{2}}{3}\sigma_x\right) d\sigma_x \ . \tag{10b}$$

Equating equations (9) and (10b) gives

$$F\left(\frac{\sqrt{2}}{3}\sigma_x\right) = f'\left(\frac{\sqrt{2}}{3}\sigma_x\right) \ . \tag{11}$$

Therefore, $F(\tau_o)$ is related to $f(\tau_o)$ as follows:

$$F(\tau_o) = f'(\tau_o) = \frac{df(\tau_o)}{d\tau_o} \ . \tag{12}$$

Making use of equation (12), equations (5a) through (5f) can be integrated to yield total permanent stresses and strains, as follows:

$$\varepsilon_x^p = \frac{f(\tau_o)}{3\tau_o}\left[\sigma_x - \frac{1}{2}(\sigma_y + \sigma_z)\right] \ , \tag{13a}$$

$$\varepsilon_y^p = \frac{f(\tau_o)}{3\tau_o}\left[\sigma_y - \frac{1}{2}(\sigma_x + \sigma_z)\right] \ , \tag{13b}$$

$$\varepsilon_z^p = \frac{f(\tau_o)}{3\tau_o}\left[\sigma_z - \frac{1}{2}(\sigma_x + \sigma_y)\right] \ , \tag{13c}$$

$$\gamma_{xy}^p = \frac{f(\tau_o)}{\tau_o}\tau_{xy} \ , \tag{13d}$$

$$\gamma_{yz}^p = \frac{f(\tau_o)}{\tau_o}\tau_{yz} \ , \tag{13e}$$

$$\gamma_{zx}^p = \frac{f(\tau_o)}{\tau_o}\tau_{zx} \ . \tag{13f}$$

These equations constitute the "incremental" or "flow" theory for plastic stress-strain relations. The actual form of the function $f(\tau_o)$ will be derived in the next section. Experimental results from references 11 and 12 indicate that incremental strain theory provides satisfactory accuracy when small strain values are considered. Thus the accuracy of equations (13a) through (13f) is considered sufficient for the analyses to be performed as part of this study.

III. ANALYSIS OF A WELD SINGLE-ZONE MATERIAL PROPERTY COUPON USING INCREMENTAL STRAIN THEORY

A nonlinear analytical method is developed in this section for a single-zone material specimen. The geometry and material of the specimen considered is presented in figure 5.

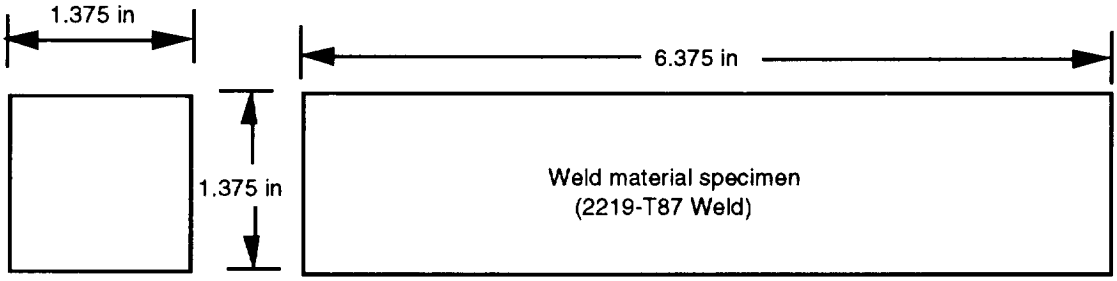

Figure 5. Geometry of single-zone specimen.

The stress-strain curve of the aluminum 2219-T87 weld based on experimental data is shown in figure 6. As indicated in figure 6, the yield stress of the weld material is approximately 10,000 lb/in^2. In order to perform the analysis required, it is first necessary to determine an expression for the function $f(\tau_o)$. This function is derived for the weld stress-strain curve in figure 6 as follows.

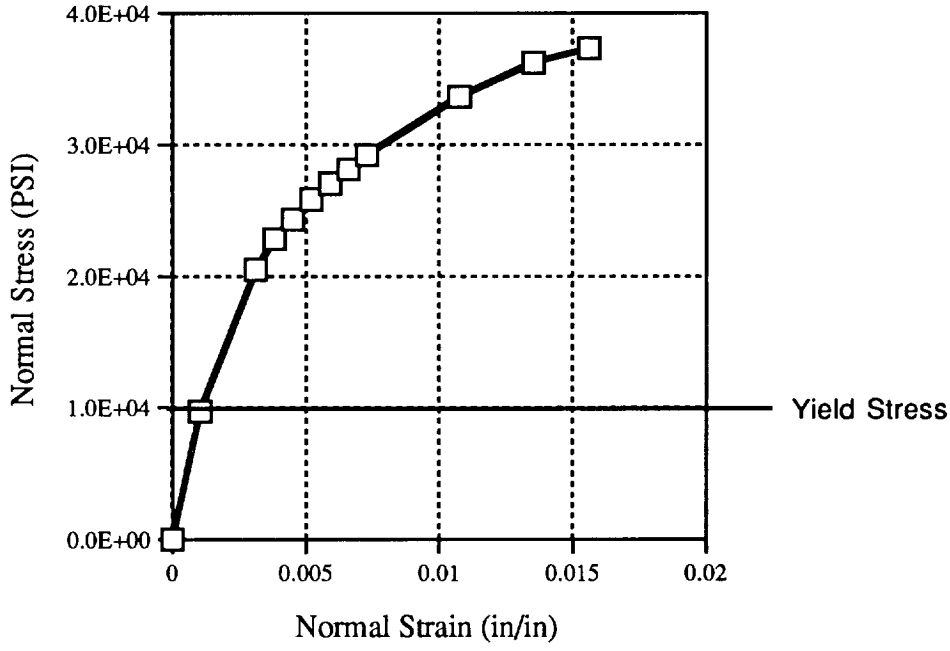

Figure 6. Weld material properties.

Following the procedure in reference 9, we define the generalized plastic strain in terms of incremental plastic strains as follows:

$$d\Gamma'' = \frac{2}{\sqrt{3}}\sqrt{d\varepsilon_x^{p2}+d\varepsilon_y^{p2}+d\varepsilon_z^{p2}+\frac{1}{2}\left(d\gamma_{xy}^{p2}+d\gamma_{yz}^{p2}+d\gamma_{zx}^{p2}\right)} \quad . \tag{14a}$$

Making use of equations (5a) through (5f) and assuming uniaxial loading, equation (14a) defines a uniaxial generalized plastic strain as follows:

$$d\Gamma_o'' = \frac{2}{\sqrt{3}}\sqrt{\left[\frac{F(\tau_o)}{3\tau_o}\sigma_x d\tau_o\right]^2+\left[\frac{F(\tau_o)}{3\tau_o}\left(-\frac{1}{2}\sigma_x\right)d\tau_o\right]^2+\left[\frac{F(\tau_o)}{3\tau_o}\left(-\frac{1}{2}\sigma_x\right)d\tau_o\right]^2} \quad . \tag{14b}$$

This reduces to

$$\sqrt{2}d\Gamma_o'' = 2\frac{F(\tau_o)}{3\tau_o}\sigma_x d\tau_o \quad . \tag{14c}$$

When $\tau_o = \frac{\sqrt{2}}{3}\sigma_x$ is substituted into the above equation the result is,

$$d\Gamma_o'' = F(\tau_o)d\tau_o \quad . \tag{14d}$$

Since, $F(\tau_o) = f'(\tau_o)$, equation (14d) becomes

$$d\Gamma_o'' = f'(\tau_o)d\tau_o \quad . \tag{14e}$$

Finally both sides of equation (14e) can be integrated to yield

$$\Gamma_o'' = \int d\Gamma_o'' = \int f'(\tau_o)d\tau_o = f(\tau_o) \quad . \tag{15}$$

Thus the quantity Γ_o'' is in fact the function $f(\tau_o)$. Continuing the procedure in reference 9, the quantity Γ_o'' is expressed in terms of plastic strain as follows:

$$\Gamma_o'' = \sqrt{2}\left(\varepsilon_x^p\right) \quad , \tag{16}$$

where,

$$\varepsilon_x^p = \varepsilon_x^{total} - \varepsilon_x^{linear} \quad . \tag{17a}$$

and

$$\varepsilon_x^{linear} = \frac{\sigma_x}{E} \quad . \tag{17b}$$

Thus, Γ_o'' is written as

$$\Gamma_o'' = \sqrt{2}\left(\varepsilon_x^{total} - \frac{\sigma_x}{E}\right) \quad . \tag{18}$$

Using the data from figure 6, the following stress-strain curve (fig. 7) is now obtained in terms of τ_o and Γ''_o:

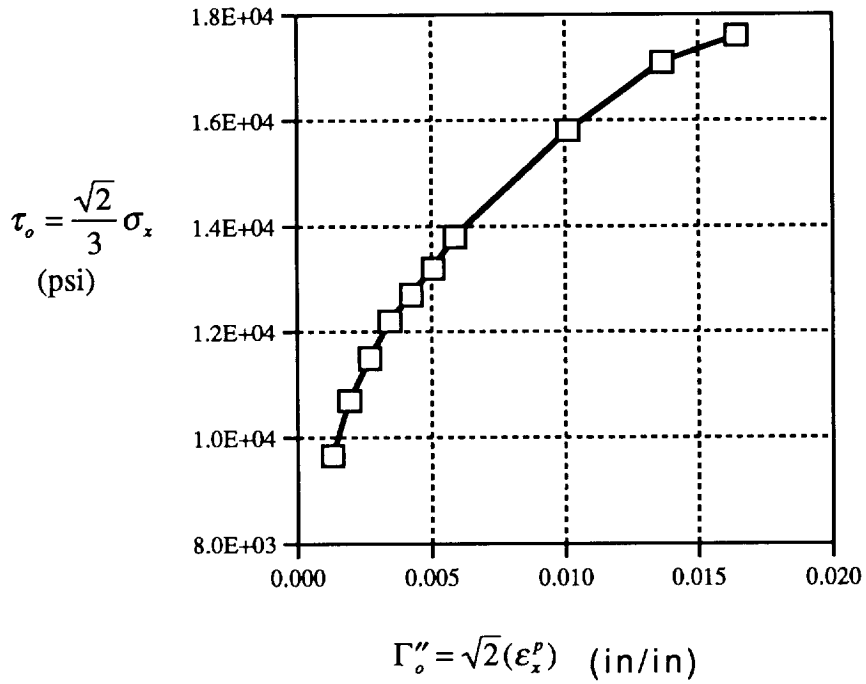

Figure 7. Generalized weld properties.

The shape of the generalized stress-strain curve suggests that τ_o can be written in terms of Γ''_o as $\tau_o = a(\Gamma''_o)^b$. As illustrated in figure 8, the log plot of the data does in fact yield a reasonably straight line. (It will be shown that the slight imperfection in the line will have negligible effects on the accuracy of the solution.)

To find the value of a and b consider the equation of a straight line, that is, $y = mx+b$. This equation can be applied to figure 8 in the form $\log(\tau_o) = b(\log(\Gamma''_o))+\log(a)$. Then the slope of the straight line in figure 8 is b and the value of $\log(\tau_0)$ when $\log(\Gamma''_o) = 0$ is $\log(a)$. Using the data in figure 8, we have

$$b = \frac{\log(17.6e3)-\log(9.66e3)}{\log(1.64e-2)-\log(1.30e-3)} = \frac{\log\left(\frac{17.6}{9.66}\right)}{\log\left(\frac{.0164}{.0013}\right)} = \frac{0.261}{1.101} = 0.2371 \ .$$

Continuing to solve for the value of a:

$$a = \frac{\tau_o}{(\Gamma''_o)^b} = \left(\frac{9.183\times10^3}{(0.0010)^{0.237}}\right) = 47.21\times10^3$$

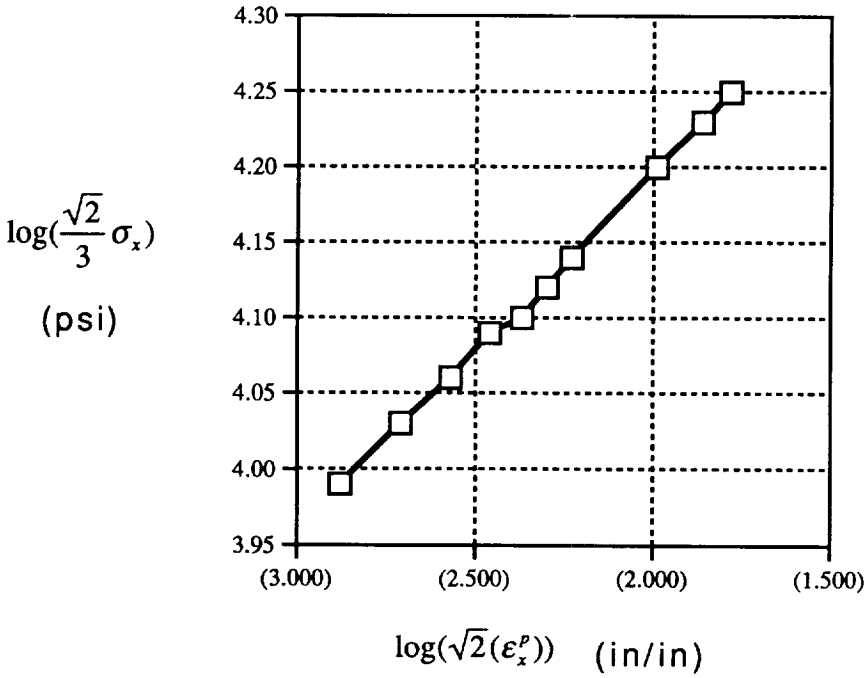

Figure 8. Log-log plot of generalized weld properties.

Thus, the equation for the generalized stress-strain curve for the weld material is:

$$\tau_o = 47.21\times10^3\left(\Gamma_o''\right)^{0.237} \quad . \tag{19}$$

Figure 9 shows a comparison of equation (19) with the test data from figure 7.

As can be seen in figure 9, the results of equation (19) compare very well with the experimental data. Following the procedure in reference 9, this equation can now be combined with the plastic stress-strain equations (13a) through (13f) as follows.

First we write:

$$\tau_o = \frac{\sqrt{2}}{3}\sigma_x = a\left(\Gamma_o''\right)^b \quad .$$

Then making use of equation (15),

$$f(\tau_o) = \Gamma_o'' = \left(\frac{\sqrt{2}}{3a}\sigma_x\right)^{\frac{1}{b}} \quad . \tag{20}$$

From which it follows that

$$\frac{f(\tau_o)}{3\tau_o} = \frac{\left(\frac{\sqrt{2}}{3a}\sigma_x\right)^{\frac{1}{b}}}{\sqrt{2}\sigma_x} \quad . \tag{21}$$

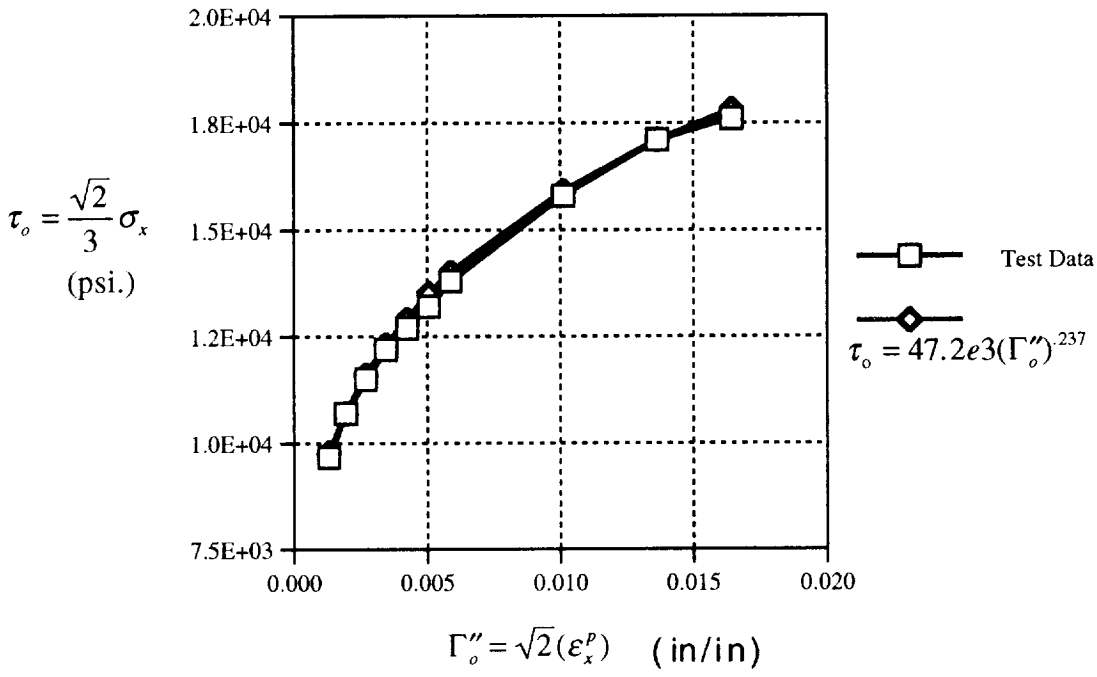

Figure 9. Comparison of test data to equation for the weld material.

Substituting equation (21) into (13a) through (13f), the plastic stress-strain equations can then be written as:

$$\varepsilon_x^p = \frac{\left(\frac{\sqrt{2}}{3a}\sigma_x\right)^{\frac{1}{b}}}{\sqrt{2}\sigma_x}\left[\sigma_x - \frac{1}{2}\left(\sigma_y+\sigma_z\right)\right], \tag{22a}$$

$$\varepsilon_y^p = \frac{\left(\frac{\sqrt{2}}{3a}\sigma_x\right)^{\frac{1}{b}}}{\sqrt{2}\sigma_x}\left[\sigma_y - \frac{1}{2}\left(\sigma_x+\sigma_z\right)\right], \tag{22b}$$

$$\varepsilon_z^p = \frac{\left(\frac{\sqrt{2}}{3a}\sigma_x\right)^{\frac{1}{b}}}{\sqrt{2}\sigma_x}\left[\sigma_z - \frac{1}{2}\left(\sigma_x+\sigma_y\right)\right], \tag{22c}$$

$$\gamma_{xy}^p = \frac{\left(\frac{\sqrt{2}}{3a}\sigma_x\right)^{\frac{1}{b}}}{\sqrt{2}\sigma_x} 3\tau_{xy}, \tag{22d}$$

$$\gamma_{yz}^{p} = \frac{\left(\frac{\sqrt{2}}{3a}\sigma_x\right)^{\frac{1}{b}}}{\sqrt{2}\sigma_x} 3\tau_{yz} \ , \tag{22e}$$

$$\gamma_{zx}^{p} = \frac{\left(\frac{\sqrt{2}}{3a}\sigma_x\right)^{\frac{1}{b}}}{\sqrt{2}\sigma_x} 3\tau_{zx} \ . \tag{22f}$$

Figure 10 compares the results of equation (22a) with $\sigma_y = \sigma_z = 0$ and the experimental stress-strain data from figure 6.

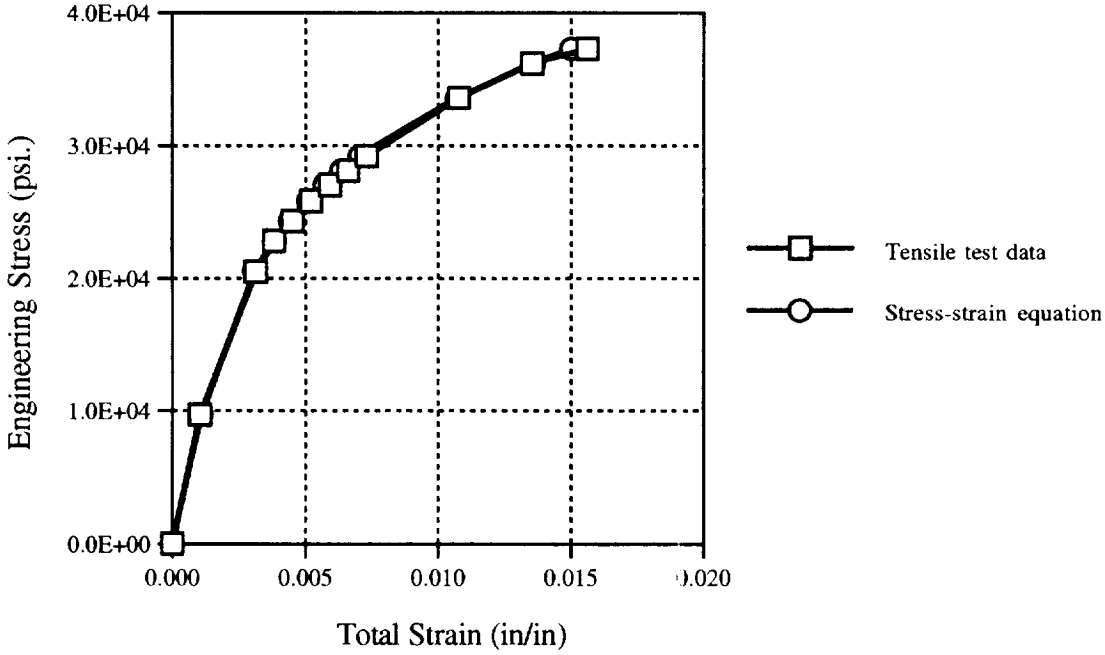

Figure 10. Comparison of test data to equation from incremental strain theory.

As can be seen in figure 10, the inelastic analytical equations compare very well to the tensile test data.

The next step is to develop a finite element model of a tensile test specimen and compare its predictions to both this 1–D analytical solution and the tensile test data. The finite-element model and the 1–D analysis will be used to develop the more complicated finite element model of the multizone test specimen in section IV.

IV. COMPUTATIONAL ANALYSIS OF A TENSILE TEST SPECIMEN

A. Introductory Comments

In correlating the analytical, computational, and test results, the goal is to systematically develop a model of a multiple-zone material weld. The single-zone model will be used as a benchmark to develop the more complex multiple-zone model. The material property data input into the finite-element code will be verified by comparison to the previously developed analytical solution and the tensile test data. The methods developed and verified for the single-zone material model will then be repeated for the multiple-zone material model.

B. The Finite-Element Model for One Material Property in the Tensile Test Specimen

The finite-element analysis program *ABAQUS* (version 5.2) is used to model the behavior of a single-zone material test specimen. The mesh geometry of the finite-element model is illustrated in figure 11.

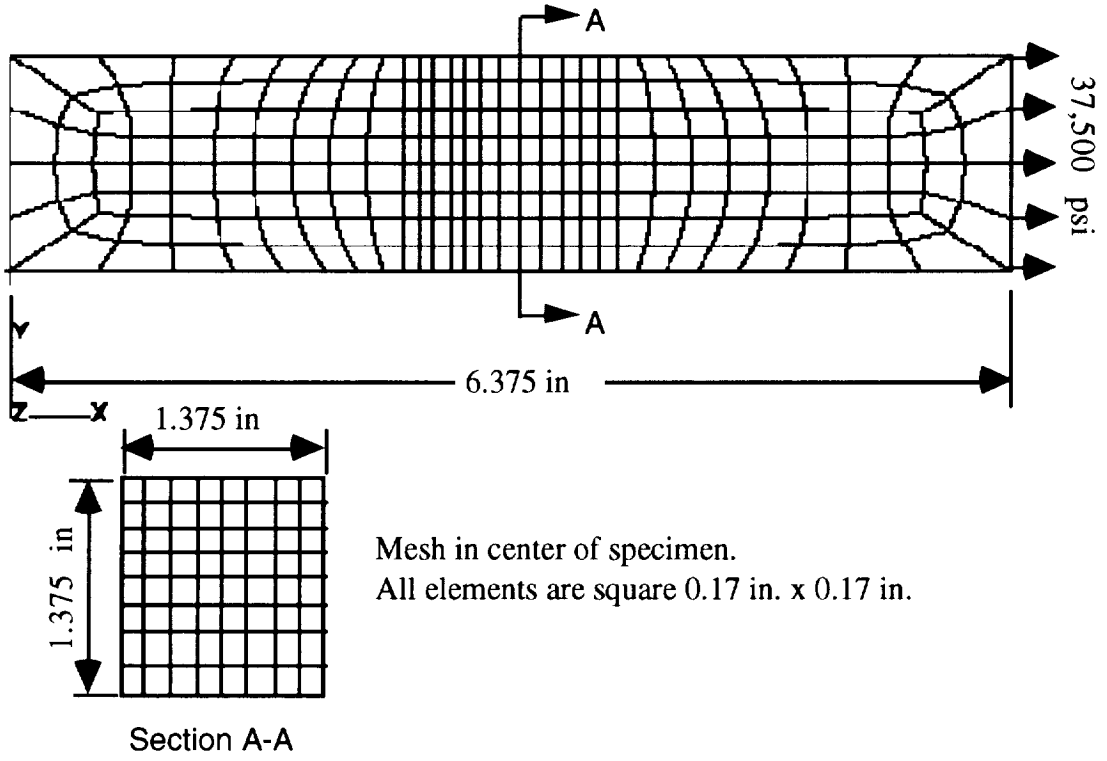

Figure 11. Finite-element model for single-zone material model.

The mesh geometry was developed to provide a high element density in the center of the specimen. Eight brick elements are used through the thickness and the width of the element; each element has an aspect ratio of 1:1. Each node at the left end is constrained in all six degrees of freedom. The loads are applied in 20 load increments from 0 to a maximum load of 37,500 lb/in^2.

The computational solution requires the development of material properties to input into the finite-element code. *ABAQUS* requires all stress and strain input data in true-stress and true-strain terms.

The engineering stress-strain curve shown in figure 12 does not give "true" deformation characteristics because it is based on the original dimensions of the test specimen. During a test, the original dimensions are continuously changing until the specimen becomes unstable and necks down before ultimate failure. The true stress value is based on the actual cross-sectional area of the specimen. The true stress versus true strain curve indicates that the stress-strain curve increases monotonically until the specimen fractures.

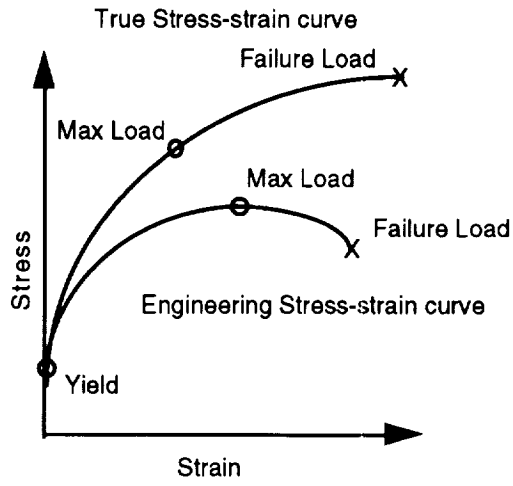

Figure 12. Stress-strain curve to illustrate true stress and true strain concept.

The true-stress equation is derived assuming the volume of the test specimen remains constant or $\varepsilon_x^p+\varepsilon_y^p+\varepsilon_z^p = 0$. This equation is only good until necking or unstable stress begins to appear in the specimen.

True stress, σ^{true}, is expressed in terms of the engineering stress, σ, by:

$$\sigma^{true} = \sigma(\varepsilon+1) \ , \tag{23a}$$

where

$$\sigma = \frac{P}{A_o} \ , \tag{23b}$$

is the engineering stress. The true strain, ε^{true}, may be determined from the engineering strain, ε, by:

$$\varepsilon^{true} = \ln(\varepsilon+1) \ . \tag{24}$$

Figure 13 shows a plot of the true stress-true strain data and the engineering stress-engineering strain for the weld material properties (fig. 6). Apparently, the difference between the "true" data and the "engineering" data is small for the strain levels considered in this study.

In addition to requiring true-stress and true-strain input data, *ABAQUS* requires that the numerical value of strain at the yield point must be zero. Therefore, the linear portion of strain must be subtracted from total strain as shown in equation (25).

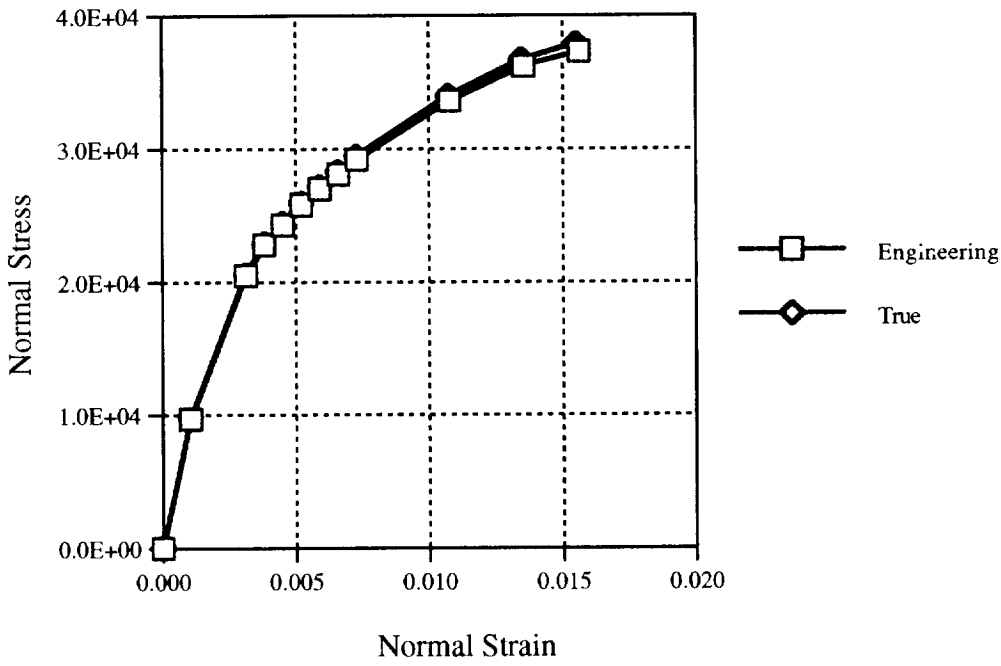

Figure 13. Comparison of true stress-strain data to engineering stress-strain data for the weld.

$$\varepsilon^{true} = \ln(\varepsilon+1)-\left(\frac{\sigma}{E}\right) . \tag{25}$$

The equations to convert the engineering stress-strain data into *ABAQUS* compatible data is given by equations (23) and (25). The *ABAQUS* **PLASTIC* solution was chosen for this analysis because it is an incremental plasticity solution in which the mechanical strain rate is decomposed into an elastic part and a plastic (inelastic) part. This solution is consistent with the incremental-strain theory discussed previously. The **PLASTIC* option is used to specify the plastic part of the material model for elastic-plastic materials that use the Mises or Hill yield surface. The *ABAQUS* input data for the **PLASTIC* option is given in table 1.

Table 1. Weld material properties (*ABAQUS* **PLASTIC* option)

Strain	Stress	True Strain	True Stress	**PLASTIC*	
0.00E+00	0	0.00E+00	0		
1.04E–03	9,700	–7.66E–07	9,710	0.00E+00	9,710
3.13E–03	20,500	9.18E–04	20,564	9.18E–04	20,564
3.82E–03	22,800	1.36E–03	22,887	1.36E–03	22,887
4.51E–03	24,300	1.89E–03	24,410	1.89E–03	24,410
5.21E–03	25,800	2.42E–03	25,934	2.42E–03	25,934
5.90E–03	27,000	2.99E–03	27,159	2.99E–03	27,159
6.60E–03	28,100	3.56E–03	28,285	3.56E–03	28,285
7.29E–03	29,200	4.13E–03	29,413	4.13E–03	29,413
1.08E–02	33,600	7.10E–03	33,962	7.10E–03	33,962
1.35E–02	36,200	9.56E–03	36,690	9.56E–03	36,690
1.56E–02	37,300	1.15E–02	37,883	1.15E–02	37,883

C. Results of the Finite-Element Analysis for a Single-Zone Material Property Test Specimen

The finite-element model is verified by a series of checks contained in the preprocessor and postprocessor code *PATRAN 3.0* . *PATRAN* is used to create and process the entire finite-element model.

The results of the finite-element model for plastic strain are compared to both analytical equation predictions and tensile test data. The analytical values are obtained by using equations (20a) through (20f), with $a = 47.21 \times 10^3$ and $b = 0.237$. Table 2 compares the analytical predictions and the *ABAQUS* results. These results are plotted in figure 14. As evident in figure 14, the agreement is excellent between the predictions of the analytical model and the predictions of the *ABAQUS* model. Furthermore, it is noted that the data in table 2 shows the constant-volume rule is maintained by the analytical solution and the computational solution. This in turn implies that the Poisson's ratio for plastic strain calculations must be 0.5.

Table 2. Comparison of analytical and computational methods.

Analytical Equations				*ABAQUS* results (Converted to English data)			
Strain *X*	Strain *Y*	Strain *Z*	$\varepsilon_x^p+\varepsilon_y^p+\varepsilon_z^p$	Strain *X*	Strain *Y*	Strain *Z*	$\varepsilon_x^p+\varepsilon_y^p+\varepsilon_z^p$
0.00E+00	0.00E+00	0.00E+00	0.0000	0.00E+00	0.00E+00	0.00E+00	0.0000
3.63E-08	-1.82E-08	-1.82E-08	0.0000	0.00E+00	0.00E+00	0.00E+00	0.0000
6.77E-07	-3.38E-07	-3.38E-07	0.0000	0.00E+00	0.00E+00	0.00E+00	0.0000
3.74E-06	-1.87E-06	-1.87E-06	0.0000	0.00E+00	0.00E+00	0.00E+00	0.0000
1.26E-05	-6.30E-06	-6.30E-06	0.0000	0.00E+00	0.00E+00	0.00E+00	0.0000
3.23E-05	-1.62E-05	-1.62E-05	0.0000	0.00E+00	0.00E+00	0.00E+00	0.0000
6.97E-05	-3.49E-05	-3.49E-05	0.0000	1.30E-04	-6.51E-05	-6.51E-05	0.0000
1.34E-04	-6.68E-05	-6.68E-05	0.0000	2.89E-04	-1.44E-04	-1.44E-04	0.0000
2.34E-04	-1.17E-04	-1.17E-04	0.0000	4.47E-04	-2.24E-04	-2.24E-04	0.0000
3.85E-04	-1.93E-04	-1.93E-04	0.0000	6.06E-04	-3.03E-04	-3.03E-04	0.0000
6.00E-04	-3.00E-04	-3.00E-04	0.0000	7.65E-04	-3.82E-04	-3.82E-04	0.0000
8.96E-04	-4.48E-04	-4.48E-04	0.0000	9.30E-04	-4.65E-04	-4.65E-04	0.0000
1.29E-03	-6.46E-04	-6.46E-04	0.0000	1.29E-03	-6.43E-04	-6.43E-04	0.0000
1.81E-03	-9.03E-04	-9.03E-04	0.0000	1.88E-03	-9.38E-04	-9.38E-04	0.0000
2.46E-03	-1.23E-03	-1.23E-03	0.0000	2.57E-03	-1.28E-03	-1.28E-03	0.0000
3.28E-03	-1.64E-03	-1.64E-03	0.0000	3.48E-03	-1.74E-03	-1.74E-03	0.0000
4.29E-03	-2.15E-03	-2.14E-03	0.0000	4.52E-03	-2.25E-03	-2.25E-03	0.0000
5.51E-03	-2.76E-03	-2.75E-03	0.0000	5.75E-03	-2.87E-03	-2.86E-03	0.0000
6.98E-03	-3.49E-03	-3.49E-03	0.0000	6.98E-03	-3.48E-03	-3.47E-03	0.0000
8.70E-03	-4.35E-03	-4.35E-03	0.0000	8.63E-03	-4.29E-03	-4.29E-03	0.0001
1.07E-02	-5.35E-03	-5.34E-03	0.0000	1.09E-02	-5.42E-03	-5.41E-03	0.0001

Figure 15 is a comparison of the tensile test data and the results from the computational analysis. The excellent agreement establishes that the method of developing the material model input for *ABAQUS* is correct.

The methods used to develop the single-zone material model will now be extended to develop a multiple-zone material model. The validity of the multiple-zone model will be determined by comparing the results of the multiple-zone model to experiment data obtained from reference 6.

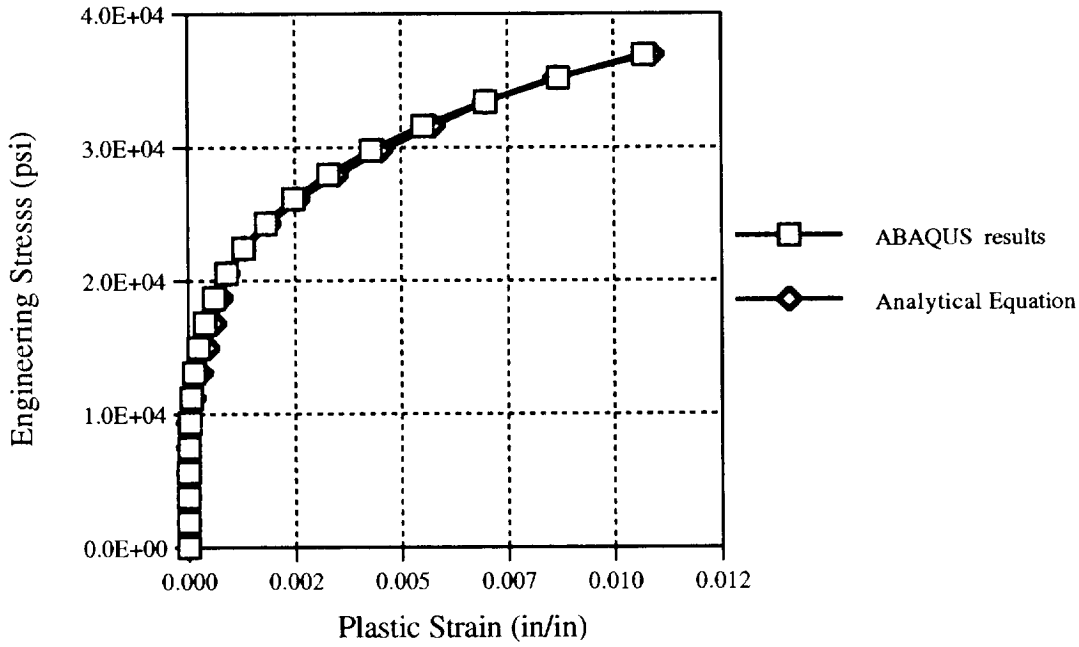

Figure 14. Comparison of computational results and analytical predictions.

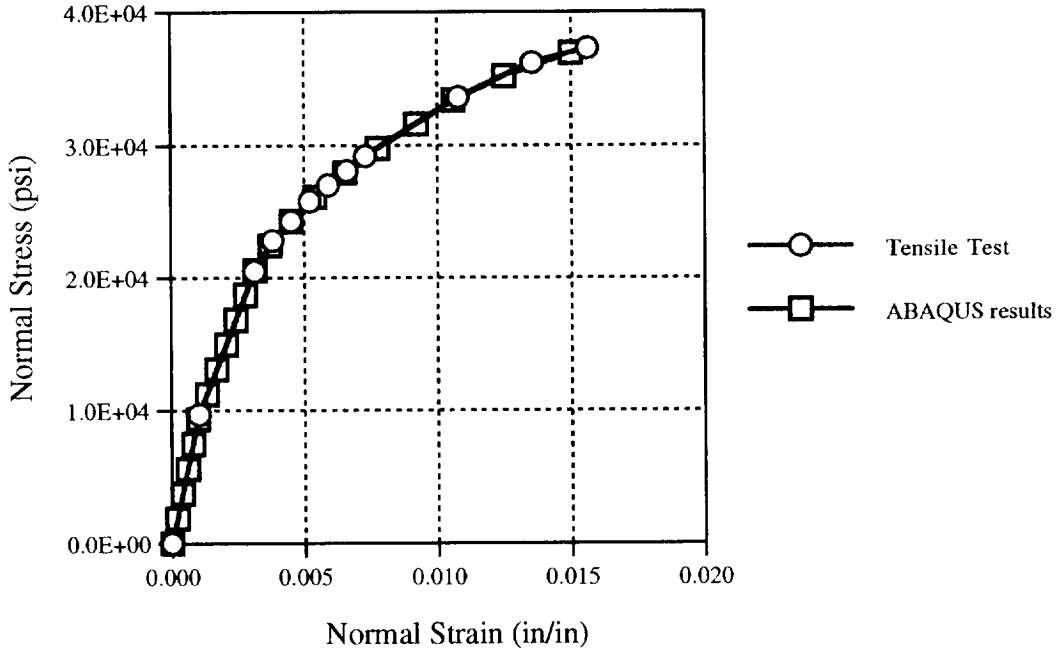

Figure 15. Comparison of computational results and tensile test results.

D. The Analysis of Multiple-Zone Material Properties in the Tensile Test Specimen

1. *Experimental Results.* The geometry of the specimen to be considered for the computational models is illustrated in figure 16. As can be seen in figure 16, the specimen can have multiple material properties.

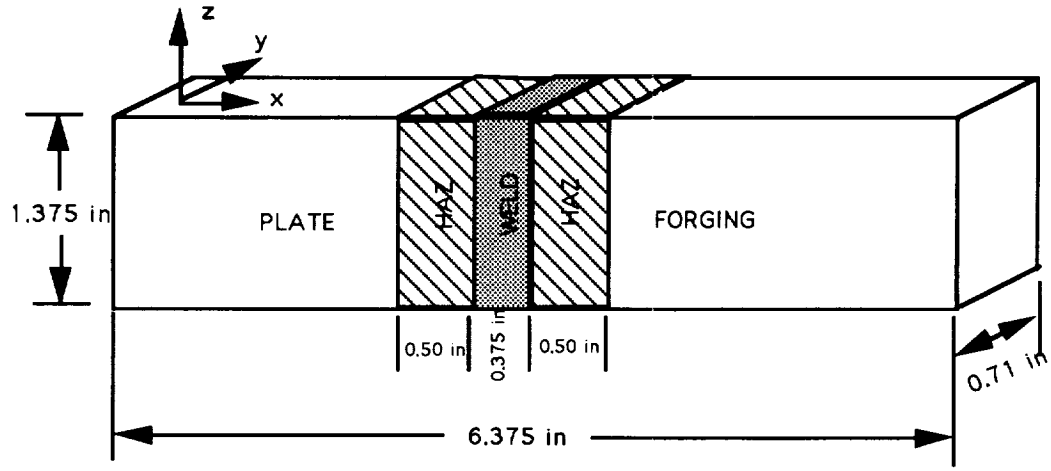

Figure 16. Geometry of multiple-zone test specimen.

The dimensions of the specimen were chosen to ensure that the plane stress ($\sigma_y = \sigma_z = 0$) condition was maintained when one material was used in the finite-element model. The nomenclature used in the development of the multiple-zone material specimen is illustrated in figure 17.

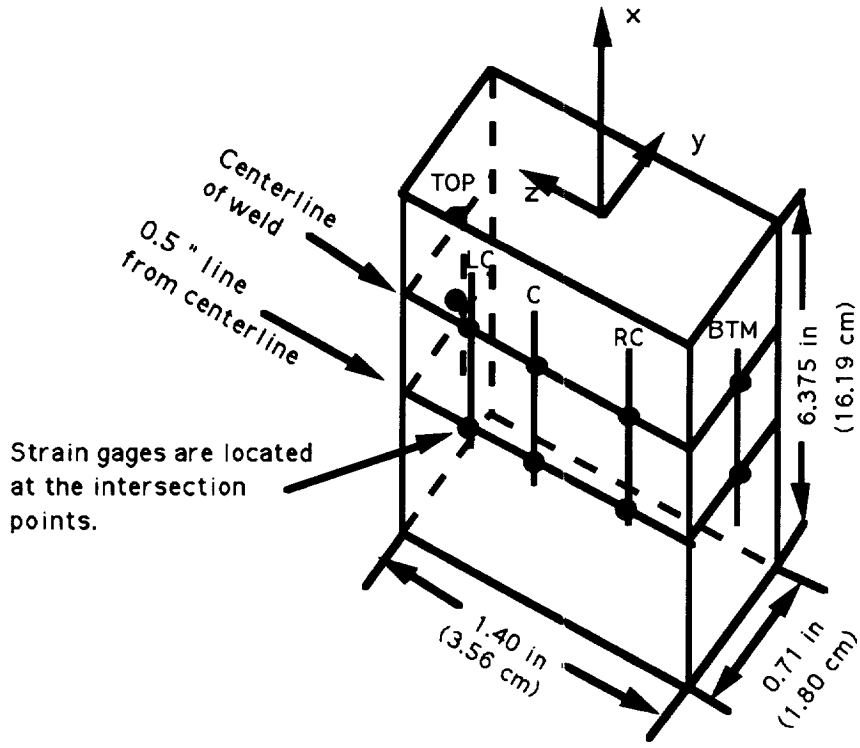

Figure 17. Strain gauge locations for the multiple-zone test specimen.

Strain gauge data was collected at points along the centerline of the weld and at points ½ inch from the centerline. The data points are referred to by the label of the intersecting lines, i.e., centerline at *C*.

Stress-strain curves were experimentally obtained for each of the intersection points shown in figure 17. Centerline curves are given in figure 18, while figure 19 shows the curves for the various locations ½ inch away from the centerline. The data represents the average of two test specimens; no visible neckdown occurred during the test and the specimens were not loaded to failure. The strain values were recorded at increasing loads during each experiment, and the corresponding stress values were obtained by dividing the load by the initial area of the specimen. It should be noted that the experimental data indicate a variation in Young's modulus across the specimen. At the center of the specimen Young's modulus corresponds to the expected value for aluminum (10.6×10^6 lb/in^2). However, at locations toward the *TOP* of the specimen Young's modulus decreases to 6.7×10^6 lb/in^2. Conversely at locations toward the *BTM* of the specimen Young's modulus increases to 15.6×10^6 lb/in^2. This is an indication that the specimens were not in a uniform state of stress. For the purposes of this investigation, the experimental data will be used as is, recognizing that the material properties for this specimen are derived under a nonuniform state of stress. The stress-strain data was converted to the input format required by *ABAQUS* using the methods benchmarked in the previous section.

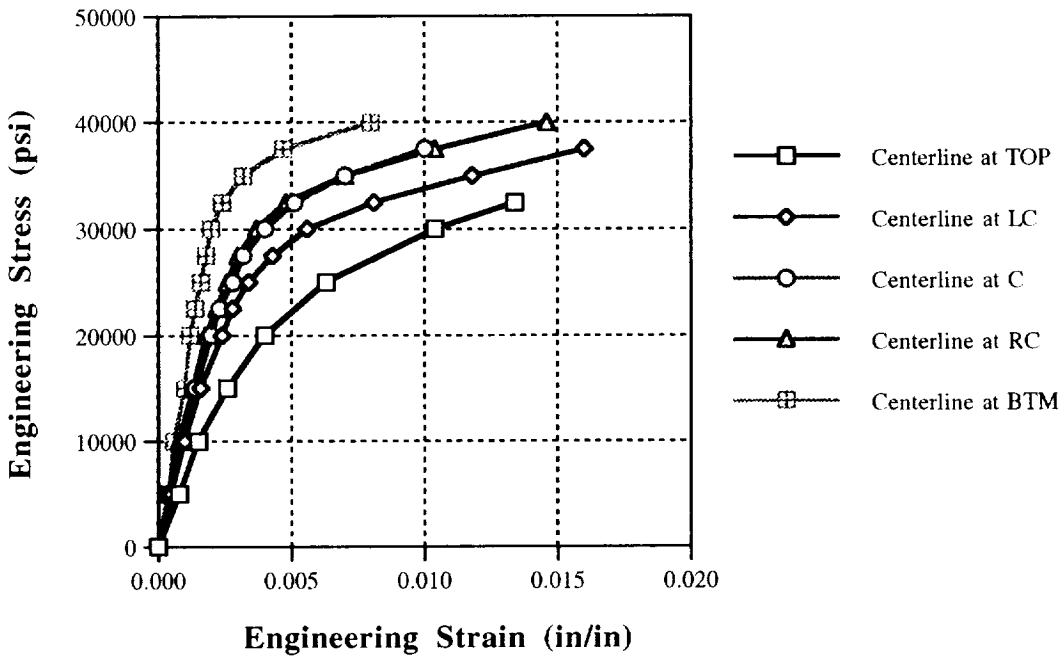

Figure 18. Experimental stress-strain curve from the multiple-zone specimen at the centerline.

The data in figure 18 indicates a large variation in response along the centerline from the *TOP* side of the specimen to the *BTM* side. In addition, the data at the centerline of the weld is different than that at the ½-in line. As can be seen in figure 19, the data at the ½-in line is more uniform than the data shown in figure 18. The material properties are expected to be more uniform at points away from the weld because eventually the data will become the uniform parent material properties. In fact, the data in figure 19 can be approximated by a single curve for stress values below 30 ksi.

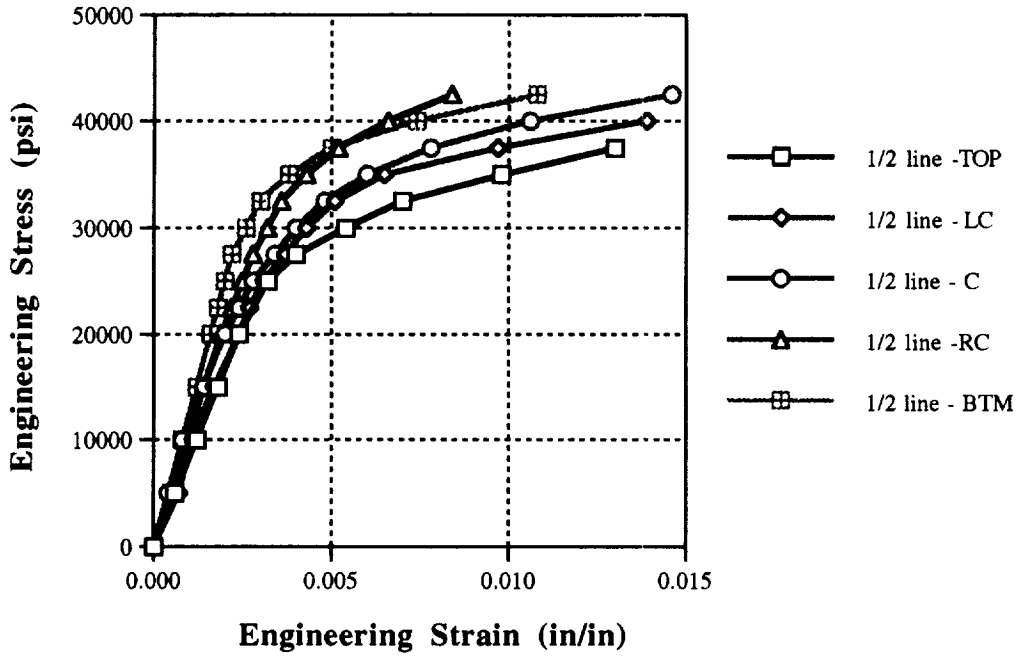

Figure 19. Experimental stress-strain curve from the multiple-zone specimen at the 1/2-in line.

2. *Finite-Element Modeling and Results for the Multiple-Zone Specimen.* The finite-element model is composed of 16 elements from the *TOP* side to the *BTM* side of the specimen. The stress-strain data for locations between those at which experimental data were obtained are given by linear interpolation of the experimental data. For example, the strain at a location between *TOP* and *LC* is calculated using the following set of equations:

$$\text{Strain} = \left[\frac{\Delta R}{R_{TOP} - R_{LC}}(N_e)\right](\varepsilon_{TOP} - \varepsilon_{LC}) \ , \tag{26a}$$

$$\text{Young's Modulus} = \left[\frac{\Delta R}{R_{TOP} - R_{LC}}(N_e)\right](E_{TOP} - E_{LC}) \ , \tag{26b}$$

where ΔR is the length between elements, N_e is the element increment number from *TOP*, and $R_{TOP} - R_{LC}$ is the length between *TOP* and *LC*. In this manner, the model provides a smooth transition between the various material properties.

The stiffness change associated with a sequential yield process induces a nonuniform stress field across the width of the specimen and produces bending in the specimen under an uniaxial loading. However, the tensile test equipment used to generate the data in figures 18 and 19 maintains alignment between the clamped and loading ends of the specimen. To numerically replicate the testing conditions, the specimen finite-element model was constrained laterally as shown in figure 20.

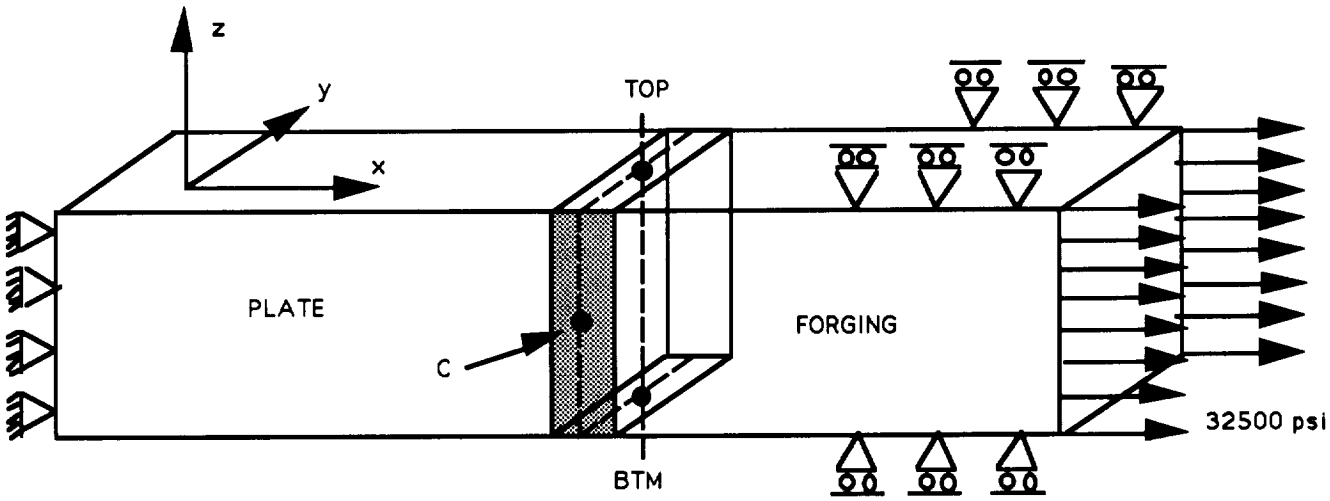

Figure 20. Illustration of the boundary conditions for the multiple-zone model.

The results of the finite-element model are compared to the experimental results across the centerline of the weld. Figures 21 through 24 compare experimental data to the finite-element predictions in the *X* direction at the *TOP*, *C*, and *BTM* locations, respectively. As can be seen in these figures, the *ABAQUS* results compared well to the experimental data in the direction of the load.

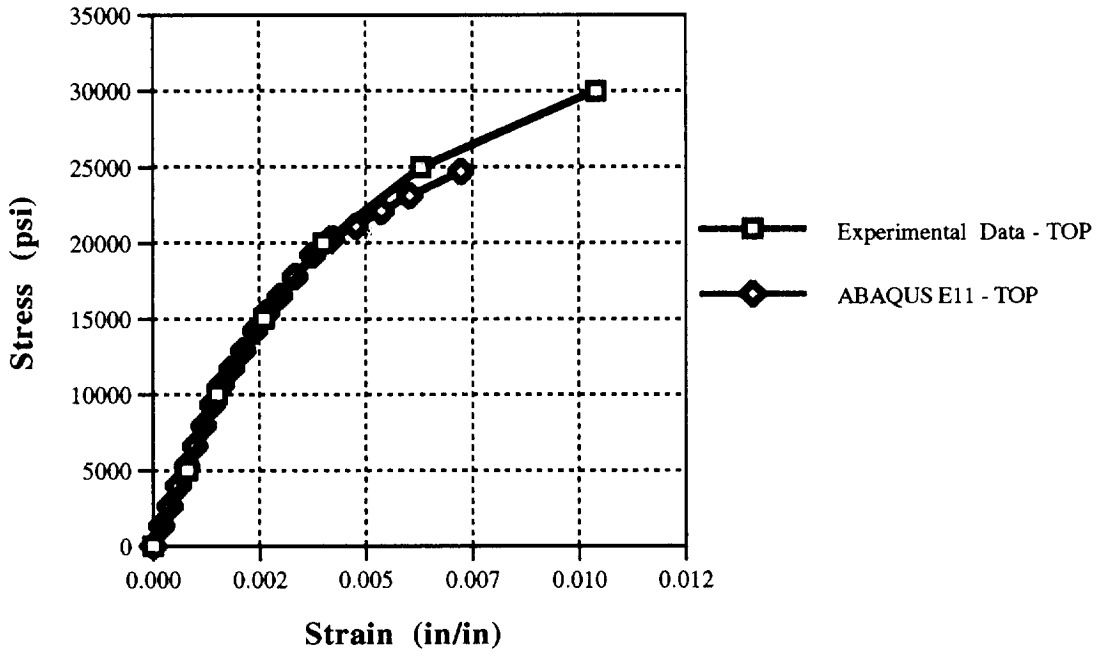

Figure 21. Comparison of *X*-direction experimental stress-strain values to finite-element results at the *TOP*.

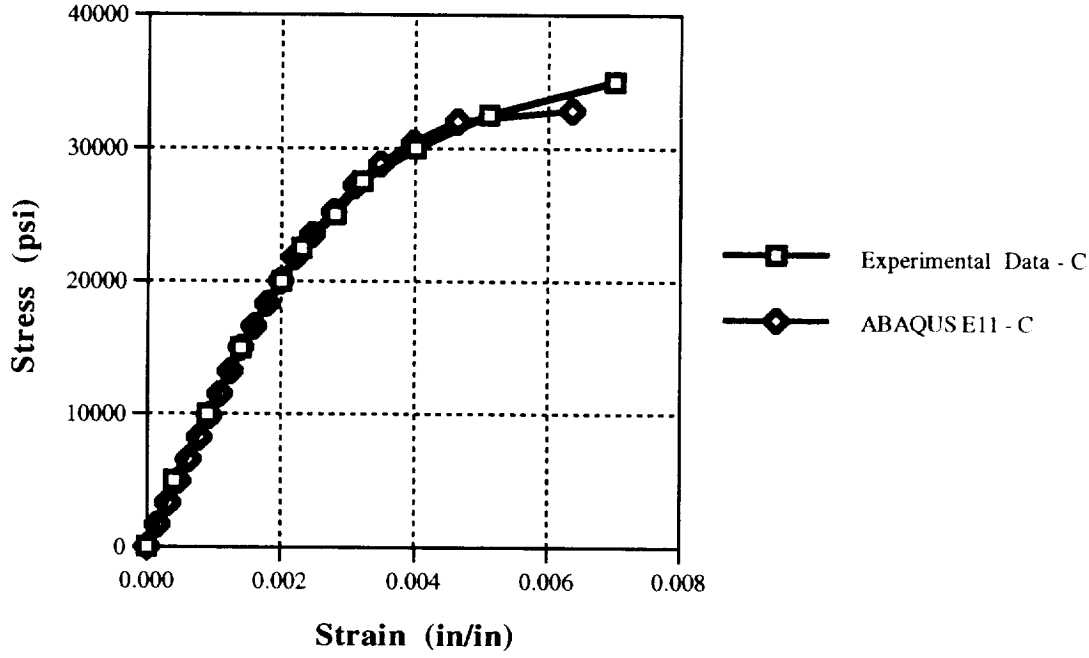

Figure 22. Comparison of *X*-direction experimental stress-strain values to finite-element results at *C*.

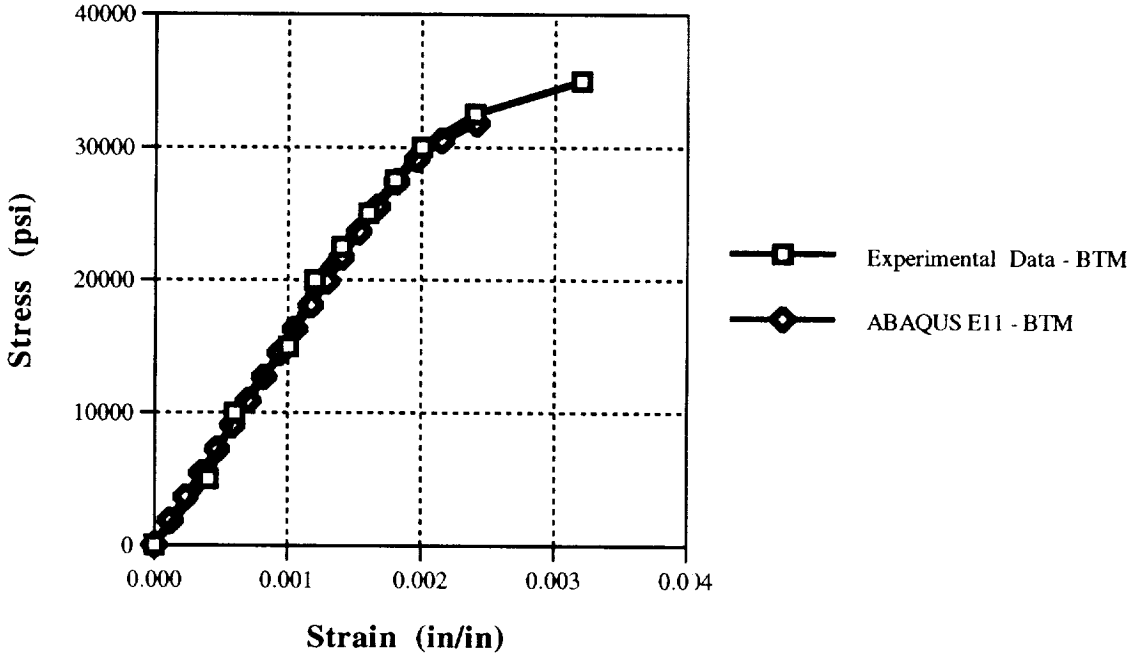

Figure 23. Comparison of *X*-direction experimental stress-strain values to finite-element results at the *BTM*.

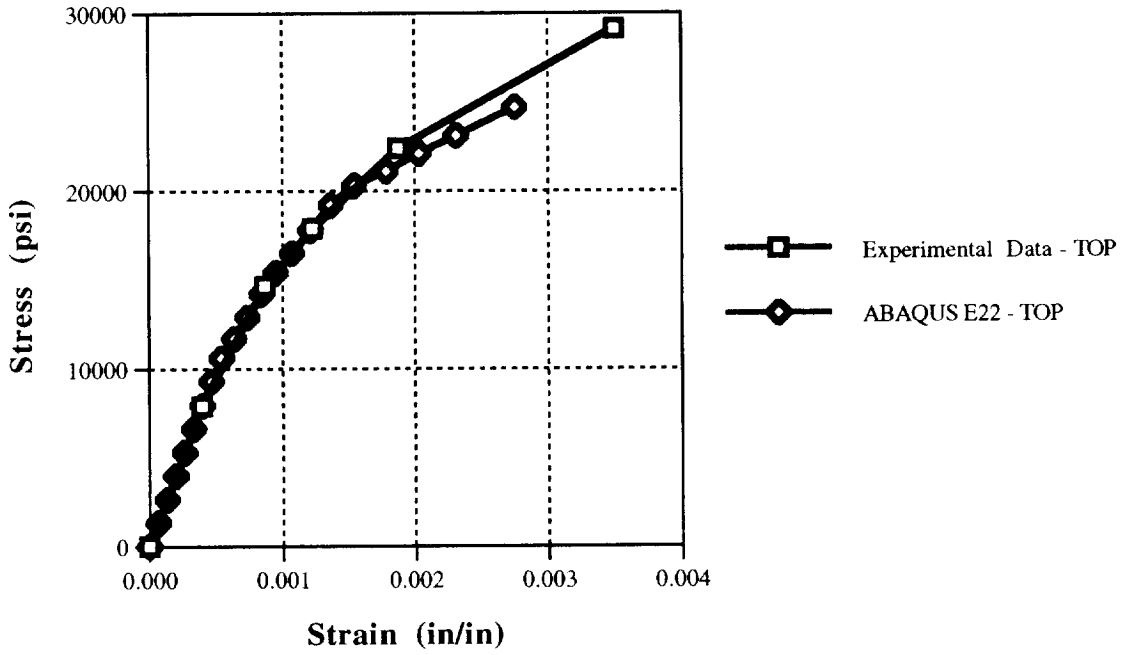

Figure 24. Comparison of *Y*-direction experimental stress-strain values to finite-element results at the *TOP*.

A comparison of the experimental results and the finite-element predictions in the *Y* direction at the *TOP* location (fig. 24), also indicates good agreement. At stress levels above 20 ksi it is noted that the model begins to slightly underpredict the experimental stress values for a given strain value.

At the *C* location, the *ABAQUS* model is in good agreement for the linear range of the response (fig. 25). However, the model overpredicts the strain at stress levels above yield. As discussed in the previous section, the incremental strain theory and *ABAQUS* both rely on the constant volume assumption, that is $\varepsilon_x^p+\varepsilon_y^p+\varepsilon_z^p = 0$; the implication of the constant volume assumption is that Poisson's ratio will be 0.5 for plastic strain. The plot of Poisson's ratio for the *C* location confirms that the Poisson's ratio is approximately 0.5 for the *ABAQUS* results in the plastic regime (fig. 26). However, in figure 27 the plot of Poisson's ratio from the experimental data indicates that Poisson's ratio is decreasing at location *C* as the load increases. This indicates that this weld specimen does not respond to applied load with constant volume deformations.

At the *BTM* location the *ABAQUS* results and the experimental results compared well in the linear region but also diverged when the response became inelastic (fig. 28). In the linear region, the slight divergence is probably caused by scatter in the experimental data.[7] However, at stress levels above yield the divergence cannot be explained by any experimental inaccuracy.[7] The experimental data in figure 27, shows that Poisson's ratio at this point in the specimen increased beyond the constant-volume assumption value of 0.5. This indicates that the deformation in the axial direction is not proportional to the deformation in the lateral directions. Physically, the specimen is deforming more in the *Y* direction than is being predicted and, as shown in figure 25, the specimen is deforming less in the *Z* direction than predicted.

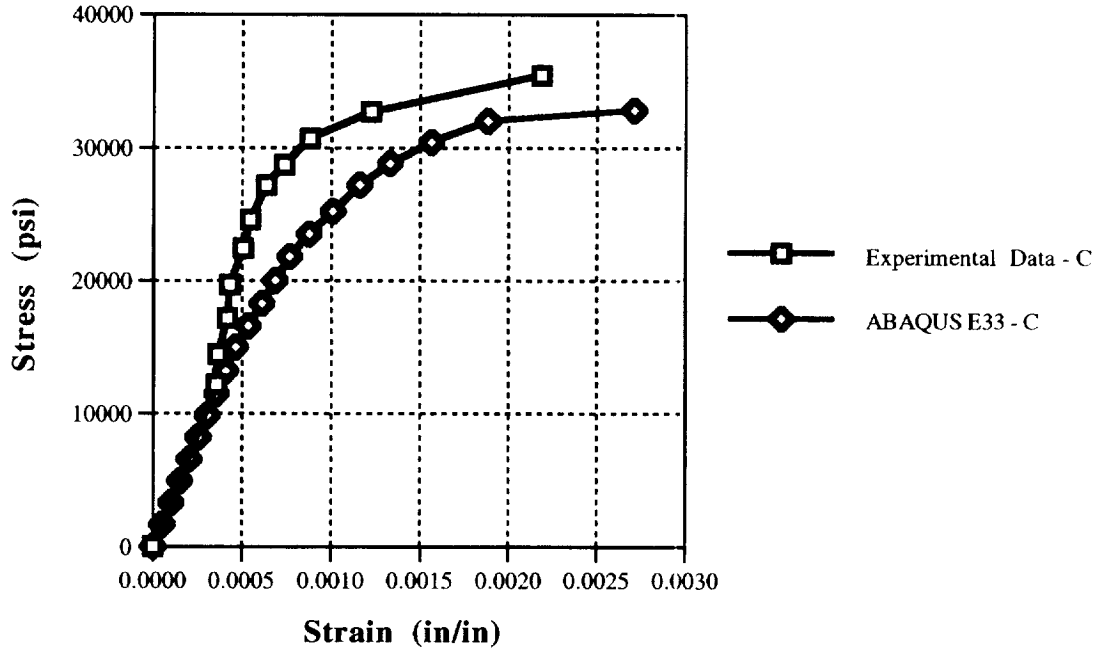

Figure 25. Comparison of *Z*-direction experimental stress-strain values to finite-element results at *C*.

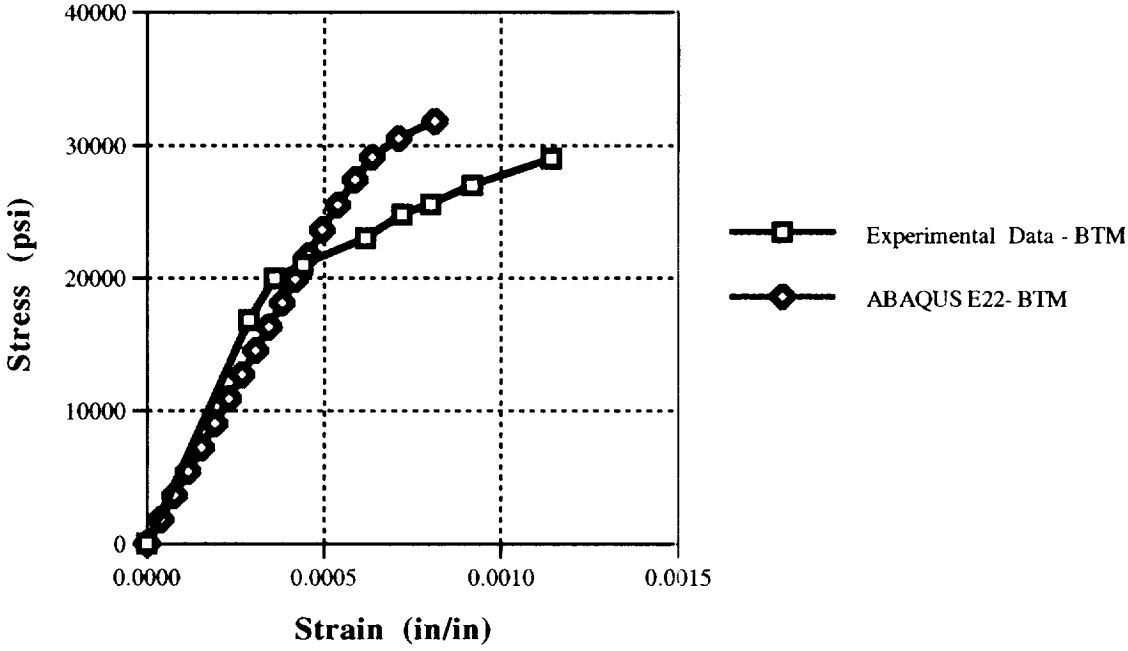

Figure 26. Poisson's ratio from the finite-element model.

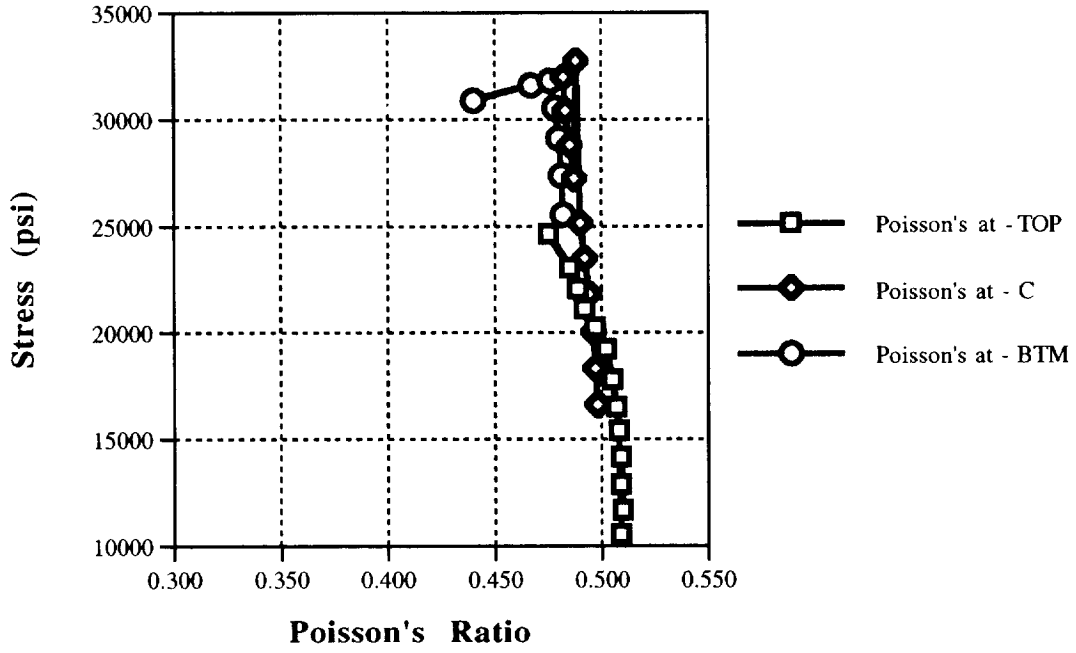

Figure 27. Poisson's ratio from experimental data.

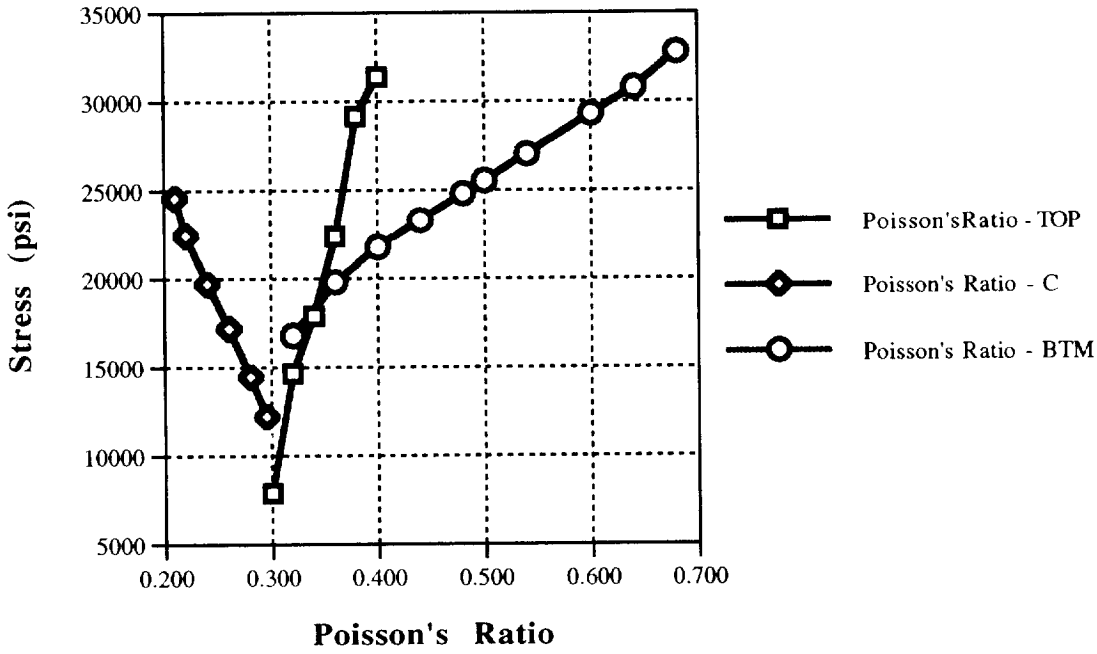

Figure 28. Comparison of *Y*-direction experimental stress-strain values to finite-element results at the *BTM*.

3. *Experimental and Computational Contour Plots.* Figure 29 shows experimental contour plots obtained during a photostress evaluation of the weld specimen.[6] The aluminum 2219-T87 weld specimens used in the photoelastic study were over 1 in thick (fig. 30). Multiple weld passes started at midthickness and alternated from one side to another in an effort to provide symmetrical material properties throughout the thickness. Figure 29 illustrates the progressive shear strain through the thickness of the weld resulting from increasingly applied axial stress. The peak strains on the outer edge due to a 24-ksi, uniaxially-applied load, indicates the presence of a residual stress induced during the weld process. As the applied stress increases, the residual stress becomes less prominent and the strain field becomes more uniform across the width of the weld.

The specimen used in the photoelastic study was instrumented with strain gauges and photoelastic stress film. Though a uniform progressive axial tension stress was externally applied on the specimen, a concentrated strain was initially noted on one side of the weld which continued to spread to the other side until the whole thickness sustained a uniform strain. In other words, the uniform axial stress unexpectedly initiated a gradient strain across the weld thickness which grew into a more uniform strain field with increasing axial stress. Hardness tests proved the initially high-strained weld side was a weaker material than the opposite side. The weaker side was also noted to have had the last weld pass.

The most likely explanation for this phenomena is that the alternating weld passes from one side to the other caused the material of the last pass to shrink and lock in strains, while cooling stresses are forcing the opposite weld side to stretch and cold work. The result is a weld with gradient material properties and an anisotropic Poisson's ratio across the thickness. It might be suspected that the very large thermal coefficient of expansion of aluminum intensifies the cold work phenomenon over steel welds. The specimens were heat treated to relieve the thermal induced strains. However, because the weld joins an aluminum plate alloy to an aluminum forging alloy, extensive heat treatment would degrade the properties of the aluminum forging.

The results of the finite-element model are presented as contour plots of strain in figures 31 through 35. These figures are included here to provide a clearer understanding of the behavior of the weld under an axial load. The deformation plot in figure 31 illustrates that the specimen model necks down at the center line of the weld. The uniform deflection across the weld is maintained by the constraints which prevent bending of the specimen. Figure 32 is the contour plot of the axial strains which illustrates the variation of the material properties from the *TOP* point to the *BTM* point. Figure 33 is a cross-sectional view of the centerline of the weld. Note that the strains are maximum over a region within the top center portion of the specimen model. The strains are not peaking across the surface of the weld where strain gauges would be located during a typical tensile test (i.e., points *LC*, *C* or *RC*). This is significant in that any subsurface flaws would be subjected to higher loads than measured by surface strain gauges. Figures 34 and 35 illustrate the strain in the *Y* direction. These figures indicate that a significant amount of shear is generated by the constraints applied to prevent bending.

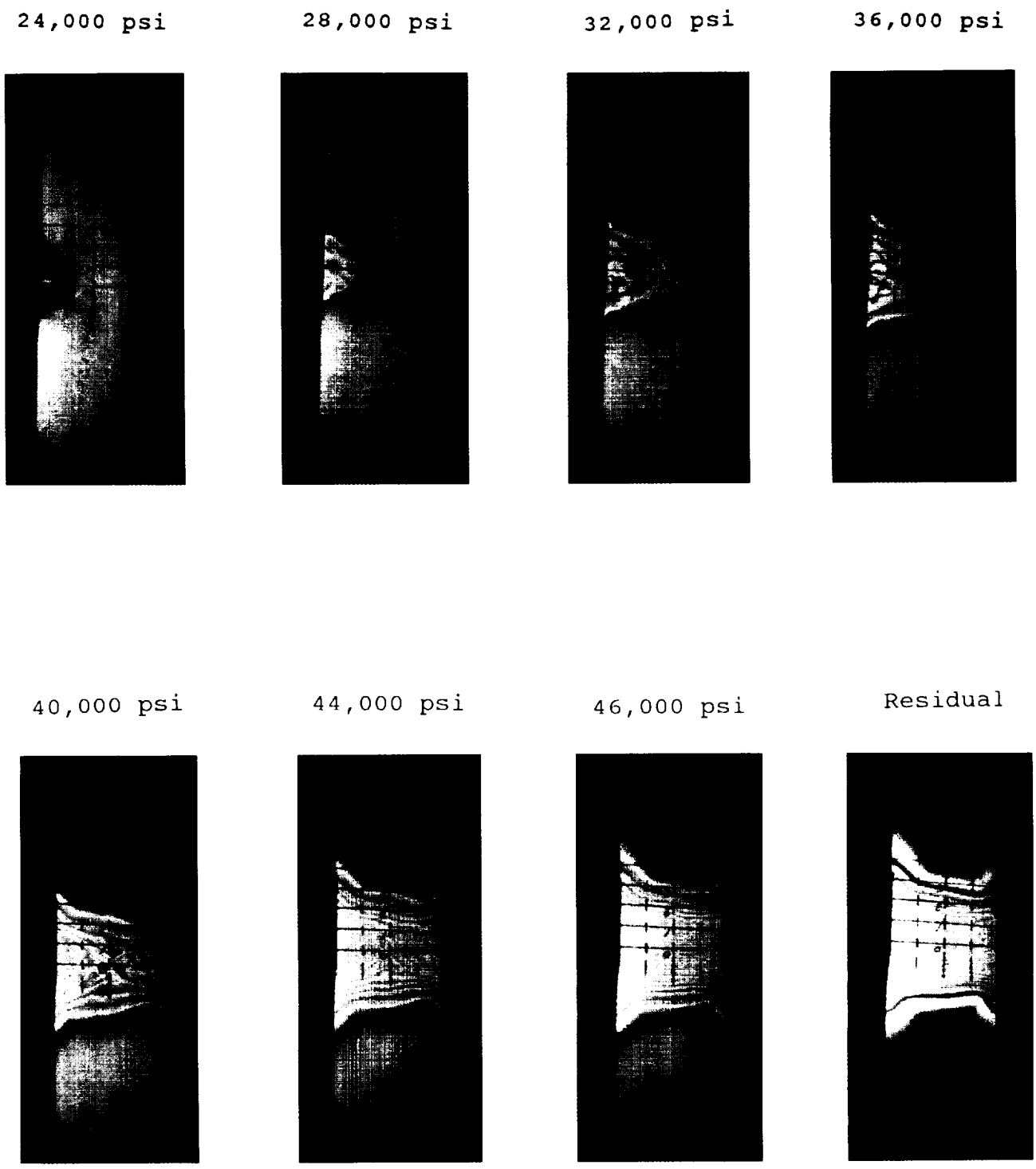

Figure 29. Photostress evaluation of a weld test specimen as the load increases (from Dr. S.C. Gambrell, University of Alabama: Report No. BER 591-97).

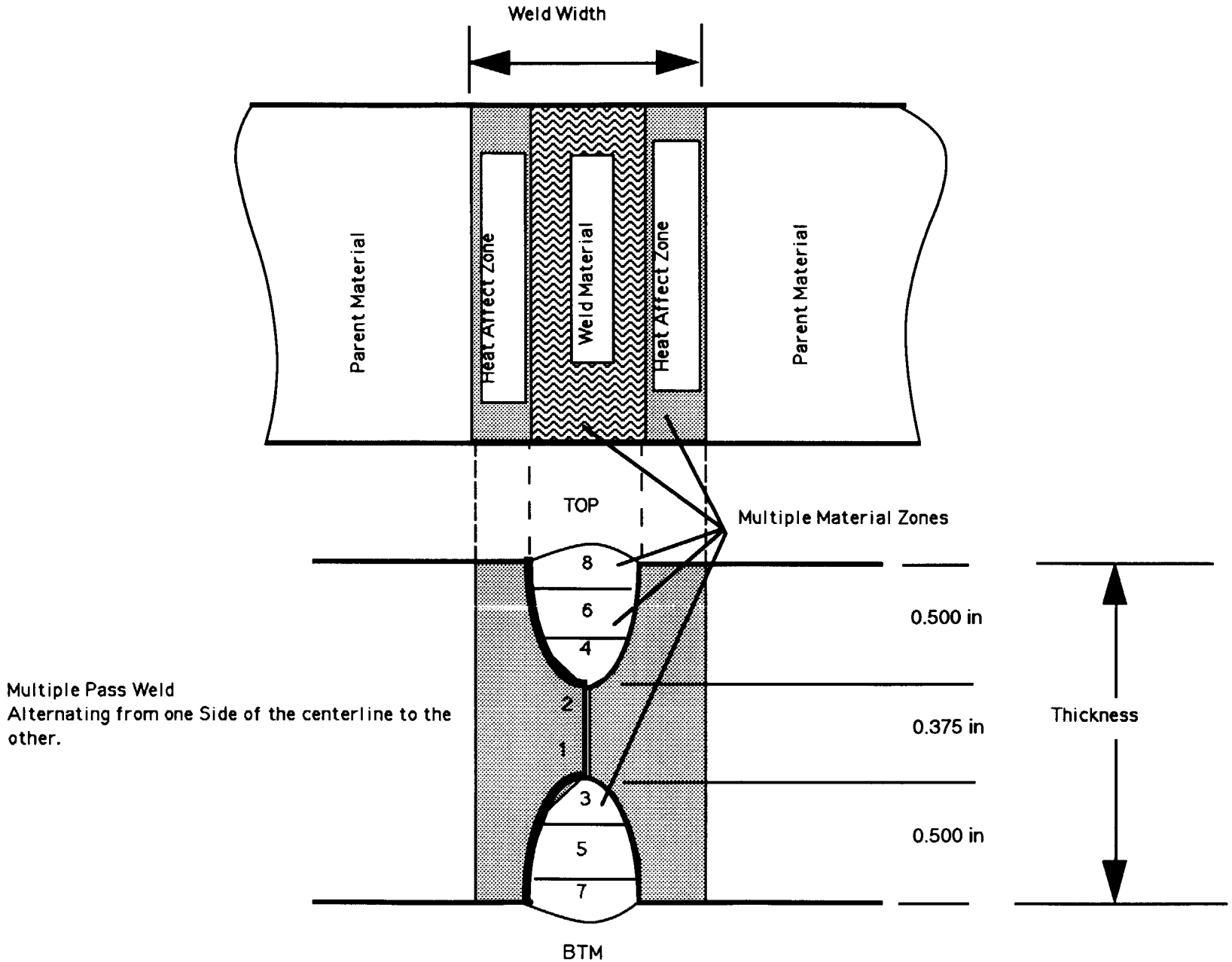

Figure 30. Cross-section view of weld.

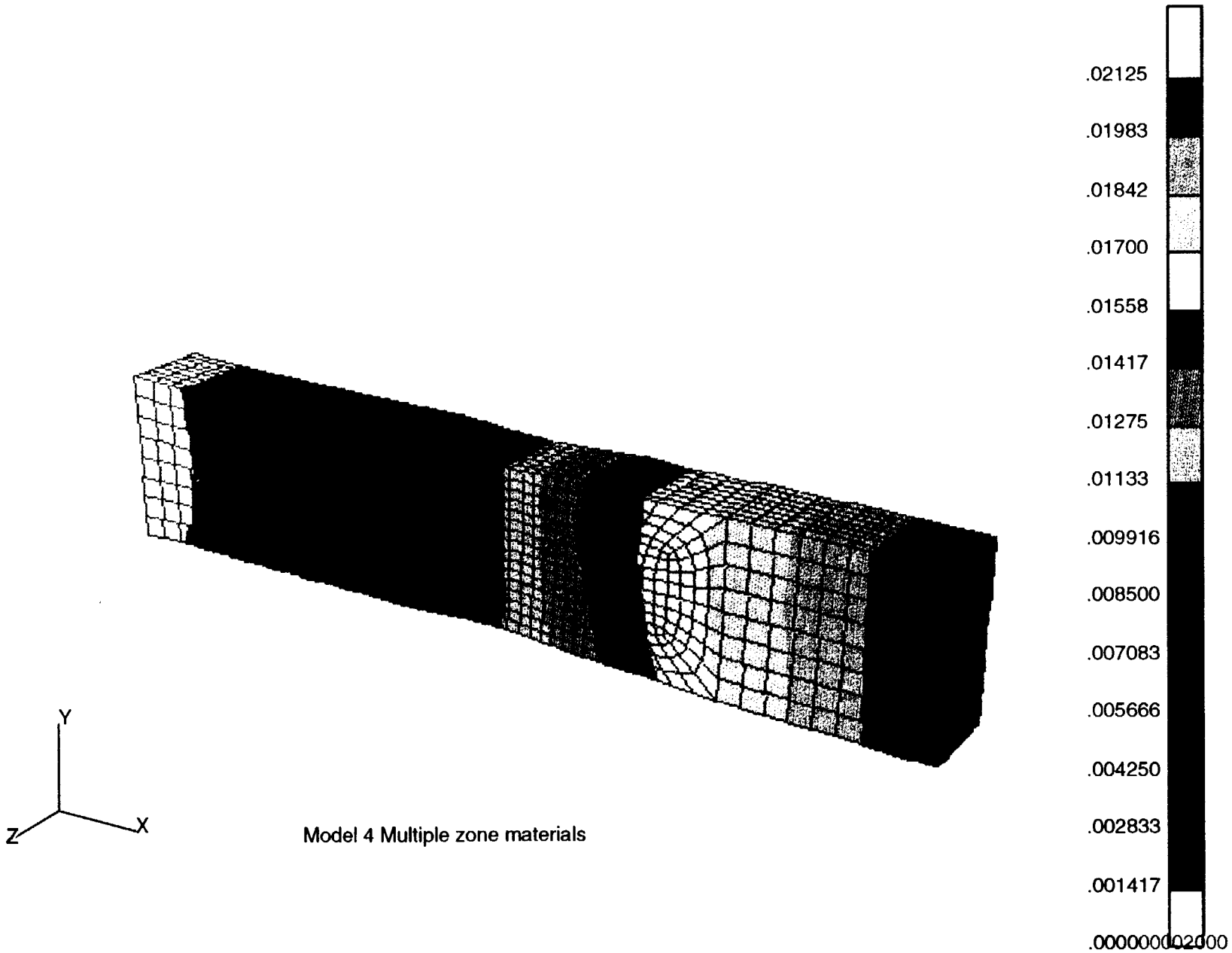

Figure 31. Contour plot of multiple-zone model; deformed shape.

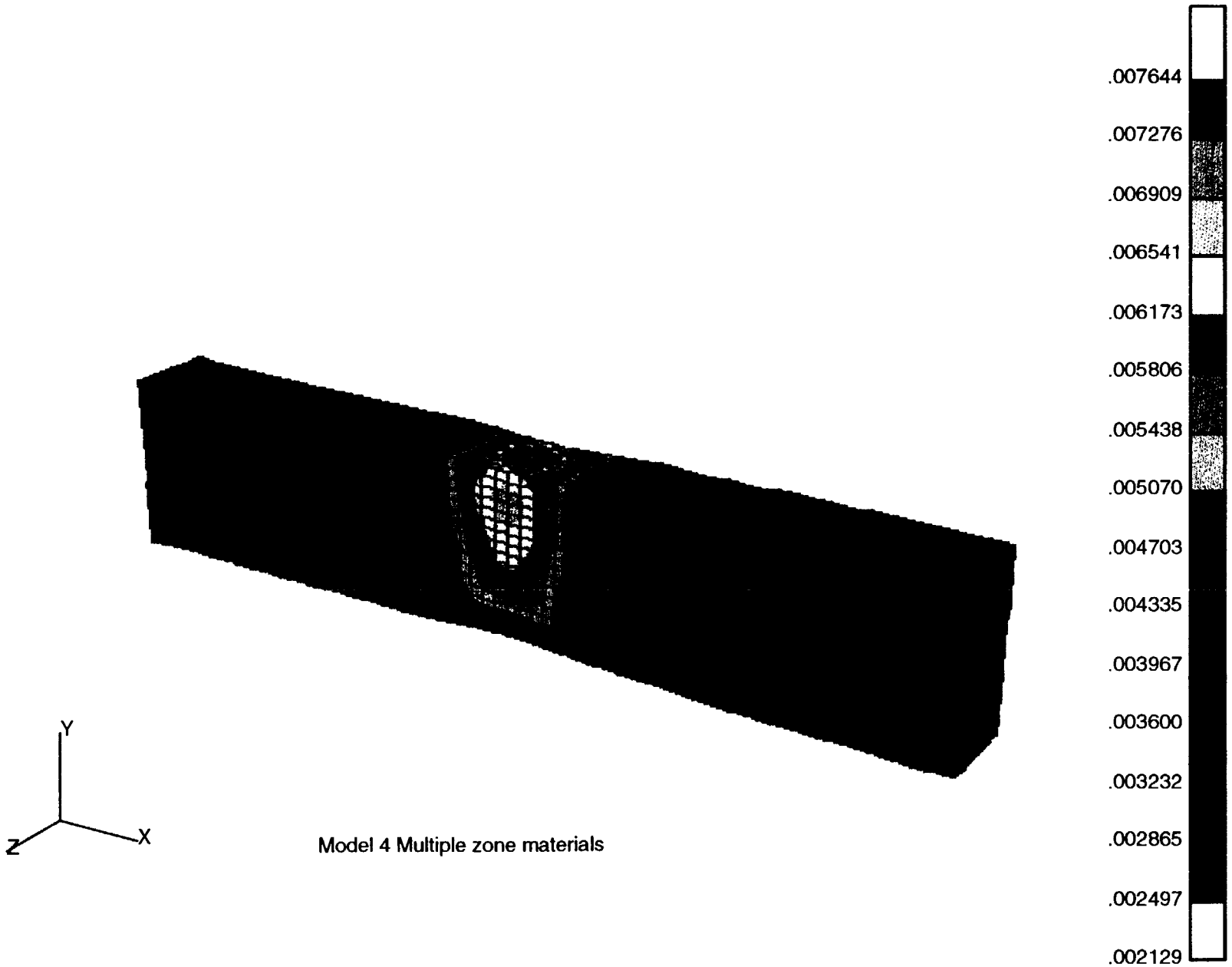

Figure 32. Contour plot of multiple-zone model; deformed shape and strain in *X* direction.

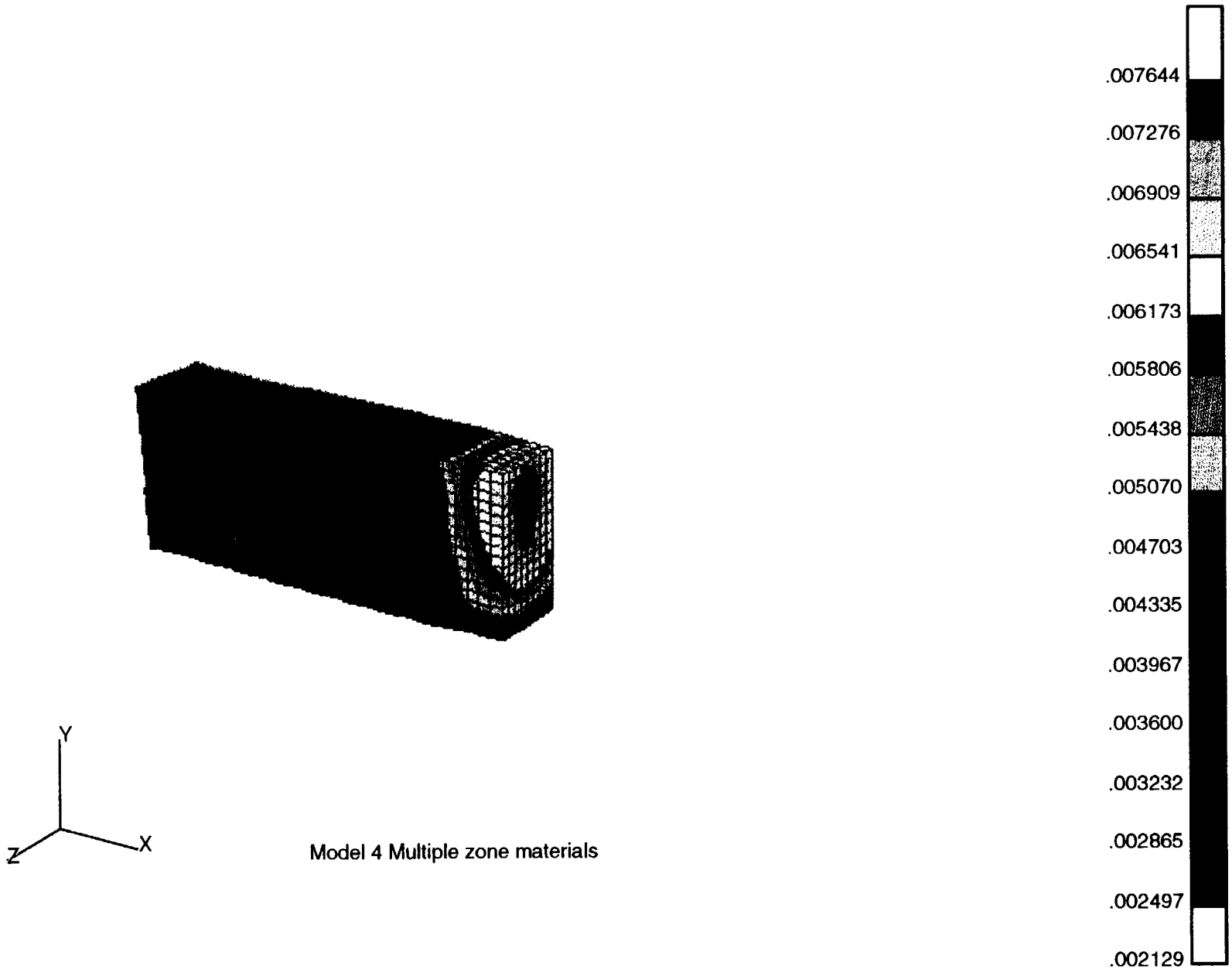

Figure 33. Contour plot of multiple-zone model; view of weld cross section; deformed shape and strain in *X* direction.

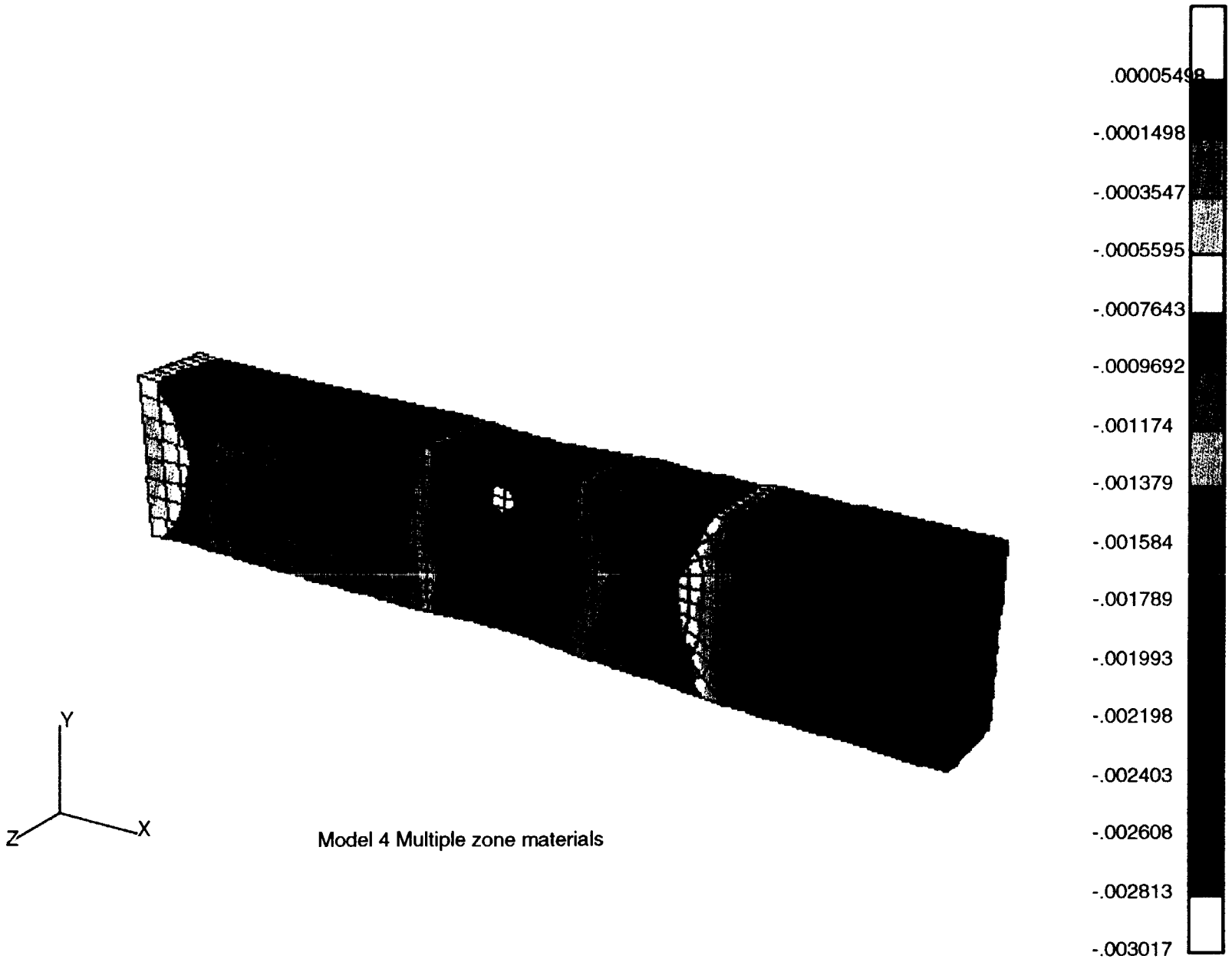

Figure 34. Contour plot of multiple-zone model; deformed shape and strain in *Y* direction.

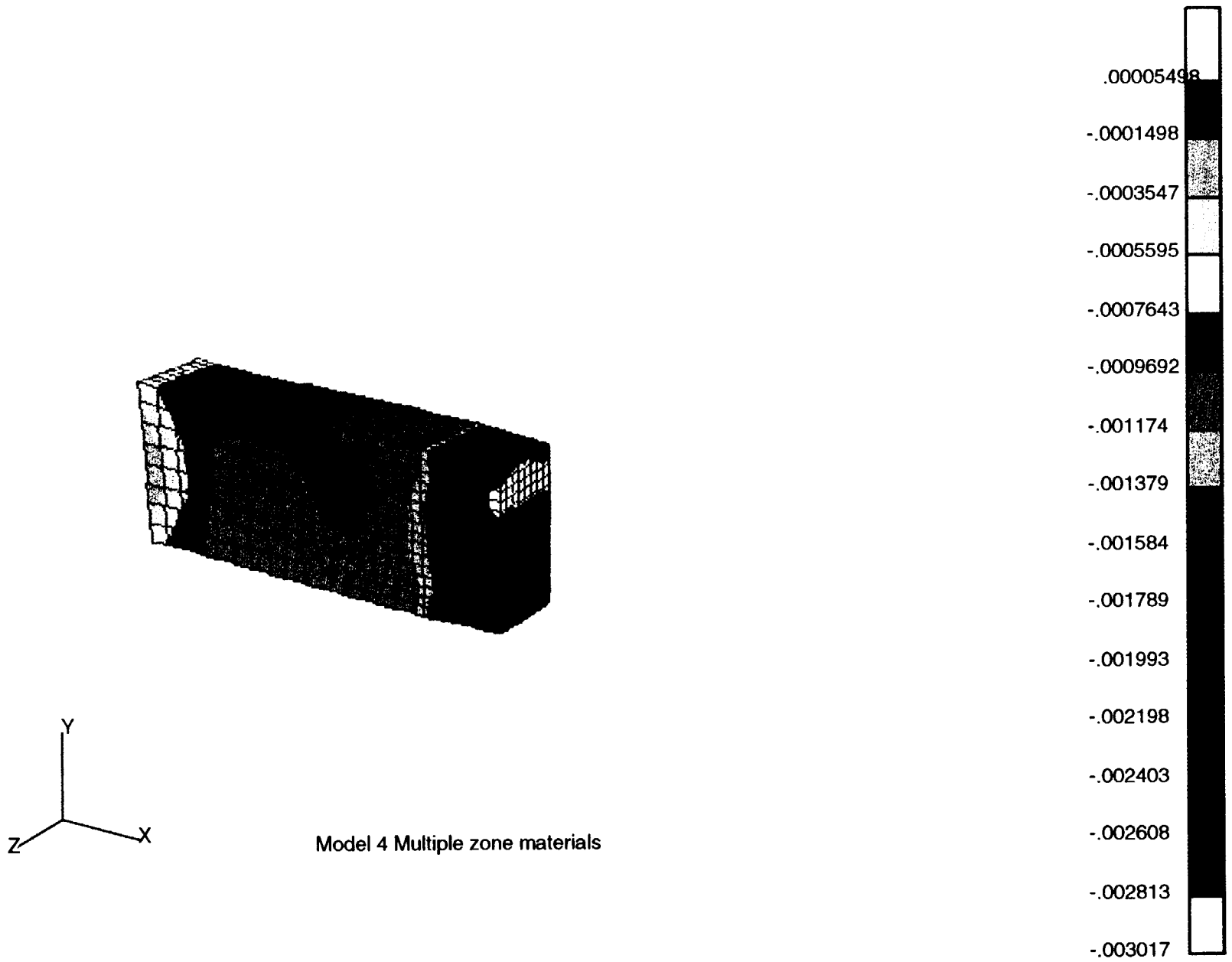

Figure 35. Contour plot of multiple-zone model; view of weld cross section; deformed shape and strain in *Y* direction.

V. CONCLUSIONS AND RECOMMENDATIONS

An approach for modeling and verifying the response of welds to uniaxially-applied loads has been successfully developed and implemented. The methods of analysis were compared to experimental results to determine the behavior and the accuracy of the analysis methods. The computational-model axial-strain predictions compared very well with longitudinal-weld experimental data but did not correlate very well with transverse strain data. Additional elements and material property inputs are not expected to increase the accuracy of the solution because the *ABAQUS* finite-element code assumes constant-volume deformation, while the experimental data indicates otherwise. The predictions of the model were significantly different from the experimental data beyond the linear elastic regime because the anisotropic nature of the weld test specimen was not included in the computational model. However, it may be possible to reformulate the 1–D stress-strain model with an appropriate Poisson's ratio, and then modify the computational model to provide more accurate weld-stress analyses.

The results obtained in this study showed a limitation in the finite-element code *ABAQUS* and illustrated the need for developing a model with an anisotropic Poisson's ratio. In addition, it demonstrated that uniaxial test data may not provide adequate material properties for thick welds. It should also be interesting to investigate the cold work phenomenon on welds of varying thickness to determine the sensitivities of the material properties to the weld thickness.

REFERENCES

1. Rybicki, E.F., and Stonesifer, R.B.: "Computation of Residual Stresses Due to Multipass Welds in Piping Systems." Journal of Pressure Vessel Technology, vol. 101, pp. 149–154, May 1979.

2. Papazoglou, V.J., and Masubuchi, K.: "Numerical Analysis of Thermal Stresses During Welding Including Phase Transformation Effects." The American Society of Mechanical Engineers, Pressure Vessels and Piping Conference, Paper No. 82-PVP-44, June 1982.

3. Agapakis, J.E. et al.: "Study of Residual Stresses and Distortion in Structural Weldments in High-Strength Steels." Final report of contract N00014-75-C-0469, M.I.T., OSP No. 82558, Massachusetts Institute of Technology, Department of Ocean Engineering, November 1982.

4. Kavikondala, K.: "Experimental-Numerical Analysis of Welded Aluminum Joints." Masters thesis, Department of Engineering Mechanics, The University of Alabama, Tuscaloosa, AL, 1993.

5. Gambrell, S.C.: "Use of Photostress Techniques to Characterize the Mechanical Behavior of Weldments." NASA/ASEE Fellowship Program, The University of Alabama, Tuscaloosa, AL, 1991.

6. Gambrell, S.C.: "Use of Photostress to Characterize the Mechanical Behavior of Weldments." The University of Alabama College of Engineering Bureau of Engineering Research, report No. 570-97, Tuscaloosa, AL, 1992.

7. Gambrell, S.C.: "Use of Photostress Techniques to Characterize the Mechanical Behavior of Weldments." The University of Alabama College of Engineering Bureau of Engineering Research, report No. 591-97, Tuscaloosa, AL, 1993.

8. Verderaime, V.: "Plate and Butt-Weld Stresses Beyond Elastic Limit, Material and Structural Modeling." NASA/Marshall Space Flight Center, TP-3075, Huntsville, AL, 1991.

9. Phillips, A.: "Introduction to Plasticity." The Ronald Press Company, NY, 1956.

10. Bridgman, P.W.: "Effects of High Hydrostatic Pressure on the Plastic Properties of Metals." Reviews of Modern Physics, vol. 17, 1945, pp. 3–14.

11. Morrison, J.L.M.: "An Experimental Investigation of Plastic Stress-Strain Relations." The Institution of Mechanical Engineering, vol. 163, 1950, pp. 1–17.

12. Ivey, H.J.: "Plastic Stress-Strain Relations and Yield Surfaces for Aluminum Alloys." Journal of Mechanical Engineering Science, vol. 3, No. 1, 1961, pp. 15–31.

APPENDIX A

REDUCTION OF EXPERIMENTAL DATA

Tensile Tests: Task 2

Normal Weld Procedure 0.71 inch x 1.4 inch
Material 2219-T87 Heat Treated

Set 1 Centerline at OD page 143

Raw Data		*Corrected Data*		*TRUE*	*TRUE*	**Plastic*
Stress	***Strain***	***Stress***	***Strain***	***Stress***	***Strain***	***Strain***
0	200	0	0.00E+00	0	0.00E+00	0.00E+00
5000	1000	5000	8.00E-04	5004	4.91E-05	0.00E+00
10000	1700	10000	1.50E-03	10015	-3.37E-06	0.00E+00
15000	2800	15000	2.60E-03	15039	3.41E-04	3.41E-04
20000	4200	20000	4.00E-03	20080	9.80E-04	9.80E-04
25000	6500	25000	6.30E-03	25158	2.51E-03	2.51E-03
30000	10600	30000	1.04E-02	30312	5.80E-03	5.80E-03
32500	13600	32500	1.34E-02	32936	8.37E-03	8.37E-03

Strain Delta = -200
Stress Delta = 0

Slope 6.67E+06

Set 2 Centerline at LC page 144

Raw Data		*Corrected Data*		*TRUE*	*TRUE*	**Plastic*
Stress	***Strain***	***Stress***	***Strain***	***Stress***	***Strain***	***Strain***
0	200	0	0.00E+00	0	0.00E+00	0.00E+00
5000	700	5000	5.00E-04	5003	-3.37E-05	0.00E+00
10000	1200	10000	1.00E-03	10010	-6.82E-05	0.00E+00
15000	1800	15000	1.60E-03	15024	-3.84E-06	0.00E+00
20000	2600	20000	2.40E-03	20048	2.59E-04	2.59E-04
22500	3000	22500	2.80E-03	22563	3.89E-04	3.89E-04
25000	3600	25000	3.40E-03	25085	7.18E-04	7.18E-04
27500	4500	27500	4.30E-03	27618	1.34E-03	1.34E-03
30000	5800	30000	5.60E-03	30168	2.37E-03	2.37E-03
32500	8300	32500	8.10E-03	32763	4.57E-03	4.57E-03
35000	12000	35000	1.18E-02	35413	7.95E-03	7.95E-03
37500	16200	37500	1.60E-02	38100	1.18E-02	1.18E-02

Strain Delta=	-200
Stress Delta=	0
Slope	9.38E+06

Set 3 Centerline at C page 145

Raw Data		*Corrected Data*		*TRUE*	*TRUE*	**Plastic*
Stress	*Strain*	*Stress*	*Strain*	*Stress*	*Strain*	*Strain*
0	0	0	0.00E+00	0	0.00E+00	0.00E+00
5000	400	5000	4.00E-04	5002	-6.69E-05	0.00E+00
10000	900	10000	9.00E-04	10009	-3.46E-05	0.00E+00
15000	1400	15000	1.40E-03	15021	-2.94E-06	0.00E+00
20000	2000	20000	2.00E-03	20040	1.28E-04	1.28E-04
22500	2300	22500	2.30E-03	22552	1.93E-04	1.93E-04
25000	2800	25000	2.80E-03	25070	4.56E-04	4.56E-04
27500	3200	27500	3.20E-03	27588	6.20E-04	6.20E-04
30000	4000	30000	4.00E-03	30120	1.18E-03	1.18E-03
32500	5100	32500	5.10E-03	32666	2.04E-03	2.04E-03
35000	7000	35000	7.00E-03	35245	3.69E-03	3.69E-03
37500	10000	37500	1.00E-02	37875	6.42E-03	6.42E-03

Strain Delta= 0
Stress Delta= 0
Slope 1.07E+07

Set 4 Centerline at RC page 146

Raw Data		*Corrected Data*		*TRUE*	*TRUE*	**Plastic*
Stress	***Strain***	***Stress***	***Strain***	***Stress***	***Strain***	***Strain***
0	-200	0	0.00E+00	0	0.00E+00	0.00E+00
5000	200	5000	4.00E-04	5002	-3.36E-05	0.00E+00
10000	600	10000	8.00E-04	10008	-6.77E-05	0.00E+00
15000	1100	15000	1.30E-03	15020	-2.53E-06	0.00E+00
20000	1600	20000	1.80E-03	20036	6.19E-05	6.19E-05
22500	2000	22500	2.20E-03	22550	2.43E-04	2.43E-04
25000	2400	25000	2.60E-03	25065	4.24E-04	4.24E-04
27500	2800	27500	3.00E-03	27583	6.05E-04	6.05E-04
30000	3500	30000	3.70E-03	30111	1.08E-03	1.08E-03
32500	4600	32500	4.80E-03	32656	1.96E-03	1.96E-03
35000	6800	35000	7.00E-03	35245	3.92E-03	3.92E-03
37500	10200	37500	1.04E-02	37890	7.06E-03	7.06E-03
40000	14400	40000	1.46E-02	40584	1.10E-02	1.10E-02

Strain Delta=	200
Stress Delta=	0
Slope	1.15E+07

Set 5 Centerline at ID page 147

Raw Data		*Corrected Data*		*TRUE*	*TRUE*	**Plastic*
Stress	*Strain*	*Stress*	*Strain*	*Stress*	*Strain*	*Strain*
0	-400	0	0.00E+00	0	0.00E+00	0.00E+00
5000	0	5000	4.00E-04	5002	7.98E-05	7.98E-05
10000	200	10000	6.00E-04	10006	-4.06E-05	0.00E+00
15000	600	15000	1.00E-03	15015	3.85E-05	3.85E-05
20000	800	20000	1.20E-03	20024	-8.23E-05	0.00E+00
22500	1000	22500	1.40E-03	22532	-4.30E-05	0.00E+00
25000	1200	25000	1.60E-03	25040	-3.84E-06	0.00E+00
27500	1400	27500	1.80E-03	27550	3.52E-05	3.52E-05
30000	1600	30000	2.00E-03	30060	7.42E-05	7.42E-05
32500	2000	32500	2.40E-03	32578	3.12E-04	3.12E-04
35000	2800	35000	3.20E-03	35112	9.48E-04	9.48E-04
37500	4300	37500	4.70E-03	37676	2.28E-03	2.28E-03
40000	7600	40000	8.00E-03	40320	5.39E-03	5.39E-03

Strain Delta=	400
Stress Delta=	0
Slope	1.56E+07

Set 6 One Half inch line at OD page 148

Raw Data		*Corrected Data*		*TRUE*	*TRUE*	**Plastic*
Stress	***Strain***	***Stress***	***Strain***	***Stress***	***Strain***	***Strain***
0	400	0	0.00E+00	0	0.00E+00	0.00E+00
5000	1000	5000	6.00E-04	5003	-5.40E-07	0.00E+00
10000	1600	10000	1.20E-03	10012	-2.16E-06	0.00E+00
15000	2200	15000	1.80E-03	15027	-4.86E-06	0.00E+00
20000	2800	20000	2.40E-03	20048	-8.64E-06	0.00E+00
25000	3600	25000	3.20E-03	25080	1.85E-04	1.85E-04
27500	4400	27500	4.00E-03	27610	6.79E-04	6.79E-04
30000	5800	30000	5.40E-03	30162	1.77E-03	1.77E-03
32500	7400	32500	7.00E-03	32728	3.05E-03	3.05E-03
35000	10200	35000	9.80E-03	35343	5.51E-03	5.51E-03
37500	13400	37500	1.30E-02	37988	8.36E-03	8.36E-03

Strain Delta=	-400
Stress Delta=	0
Slope	8.33E+06

Set 7 Half Inch Line at LC page 149

Raw Data		*Corrected Data*		*TRUE*	*TRUE*	**Plastic*
Stress	***Strain***	***Stress***	***Strain***	***Stress***	***Strain***	***Strain***
0	100	0	0.00E+00	0	0.00E+00	0.00E+00
5000	800	5000	7.00E-04	5004	1.33E-04	1.33E-04
10000	1200	10000	1.10E-03	10011	-3.52E-05	0.00E+00
15000	1800	15000	1.70E-03	15026	-4.33E-06	0.00E+00
20000	2500	20000	2.40E-03	20048	1.25E-04	1.25E-04
22500	2800	22500	2.70E-03	22561	1.39E-04	1.39E-04
25000	3200	25000	3.10E-03	25078	2.53E-04	2.53E-04
27500	3800	27500	3.70E-03	27602	5.65E-04	5.65E-04
30000	4400	30000	4.30E-03	30129	8.76E-04	8.76E-04
32500	5200	32500	5.10E-03	32666	1.38E-03	1.38E-03
35000	6600	35000	6.50E-03	35228	2.49E-03	2.49E-03
37500	9800	37500	9.70E-03	37864	5.36E-03	5.36E-03
40000	14000	40000	1.39E-02	40556	9.21E-03	9.21E-03

Strain Delta=	-100
Stress Delta=	0
Slope	8.82E+06

Set 8 Half Inch Line at C page 150

Raw Data		*Corrected Data*		*TRUE*	*TRUE*	**Plastic*
Stress	***Strain***	***Stress***	***Strain***	***Stress***	***Strain***	***Strain***
0	0	0	0.00E+00	0	0.00E+00	0.00E+00
5000	400	5000	4.00E-04	5002	-6.69E-05	0.00E+00
10000	800	10000	8.00E-04	10008	-1.34E-04	0.00E+00
15000	1400	15000	1.40E-03	15021	-2.94E-06	0.00E+00
20000	2000	20000	2.00E-03	20040	1.28E-04	1.28E-04
22500	2400	22500	2.40E-03	22554	2.92E-04	2.92E-04
25000	2800	25000	2.80E-03	25070	4.56E-04	4.56E-04
27500	3400	27500	3.40E-03	27594	8.19E-04	8.19E-04
30000	4000	30000	4.00E-03	30120	1.18E-03	1.18E-03
32500	4800	32500	4.80E-03	32656	1.74E-03	1.74E-03
35000	6000	35000	6.00E-03	35210	2.70E-03	2.70E-03
37500	7800	37500	7.80E-03	37793	4.24E-03	4.24E-03
40000	10600	40000	1.06E-02	40424	6.77E-03	6.77E-03
42500	14600	42500	1.46E-02	43121	1.05E-02	1.05E-02

Strain Delta=	0
Stress Delta=	0
Slope	1.07E+07

Set 9 Half Inch Line at RC page 151

Raw Data		*Corrected Data*		*TRUE*	*TRUE*	**Plastic*
Stress	***Strain***	***Stress***	***Strain***	***Stress***	***Strain***	***Strain***
0	-400	0	0.00E+00	0	0.00E+00	0.00E+00
5000	200	5000	6.00E-04	5003	1.11E-04	1.11E-04
10000	600	10000	1.00E-03	10010	2.07E-05	2.07E-05
15000	1000	15000	1.40E-03	15021	-6.97E-05	0.00E+00
20000	1500	20000	1.90E-03	20038	-6.11E-05	0.00E+00
22500	1800	22500	2.20E-03	22550	-7.26E-06	0.00E+00
25000	2100	25000	2.50E-03	25063	4.63E-05	4.63E-05
27500	2400	27500	2.80E-03	27577	9.97E-05	9.97E-05
30000	2800	30000	3.20E-03	30096	2.52E-04	2.52E-04
32500	3200	32500	3.60E-03	32617	4.04E-04	4.04E-04
35000	3900	35000	4.30E-03	35151	8.54E-04	8.54E-04
37500	4800	37500	5.20E-03	37695	1.50E-03	1.50E-03
40000	6200	40000	6.60E-03	40264	2.64E-03	2.64E-03
42500	8000	42500	8.40E-03	42857	4.17E-03	4.17E-03

Strain Delta=	400
Stress Delta=	0
Slope	1.02E+07

Set 10 Half Inch Line at ID page 152

Raw Data		*Corrected Data*		*TRUE*	*TRUE*	**Plastic*
Stress	***Strain***	***Stress***	***Strain***	***Stress***	***Strain***	***Strain***
0	-400	0	0.00E+00	0	0.00E+00	0.00E+00
5000	100	5000	5.00E-04	5003	9.97E-05	9.97E-05
10000	400	10000	8.00E-04	10008	-9.60E-07	0.00E+00
15000	800	15000	1.20E-03	15018	-2.16E-06	0.00E+00
20000	1200	20000	1.60E-03	20032	-3.84E-06	0.00E+00
22500	1400	22500	1.80E-03	22541	-4.86E-06	0.00E+00
25000	1600	25000	2.00E-03	25050	-6.00E-06	0.00E+00
27500	1800	27500	2.20E-03	27561	-7.26E-06	0.00E+00
30000	2200	30000	2.60E-03	30078	1.90E-04	1.90E-04
32500	2600	32500	3.00E-03	32598	3.88E-04	3.88E-04
35000	3400	35000	3.80E-03	35133	9.82E-04	9.82E-04
37500	4600	37500	5.00E-03	37688	1.97E-03	1.97E-03
40000	7000	40000	7.40E-03	40296	4.15E-03	4.15E-03
42500	10400	42500	1.08E-02	42959	7.31E-03	7.31E-03

Strain Delta=	400
Stress Delta=	0
Slope	1.25E+07

APPENDIX B

ABAQUS MATERIALS PROPERTY INPUT

```
** Material Properties Input 10/7/93
*SOLID SECTION, ELSET=PID17, MATERIAL=PLATE
*MATERIAL, NAME=PLATE
*ELASTIC
10.8E6,0.33
*SOLID SECTION, ELSET=PID18, MATERIAL=FORGING
*MATERIAL, NAME=FORGING
*ELASTIC
10.8E6,0.33
*SOLID SECTION, ELSET=PID10, MATERIAL=MID10
*MATERIAL, NAME=MID10
*ELASTIC
6.67E6,0.33
*PLASTIC
10000, 0.00E+00
15000, 3.41E-04
20000, 9.80E-04
30000, 5.80E-03
32500, 8.37E-03
*SOLID SECTION, ELSET=PID11, MATERIAL=MID11
*MATERIAL, NAME=MID11
*ELASTIC
7.22E6,0.33
*PLASTIC
10000,0.00E+00
15000,2.84E-04
20000,8.17E-04
30000,4.84E-03
32500,6.98E-03
*SOLID SECTION, ELSET=PID12, MATERIAL=MID12
*MATERIAL, NAME=MID12
*ELASTIC
7.5E6,0.33
*PLASTIC
10000, 0.00E+00
15000, 2.28E-04
20000, 6.55E-04
30000, 3.87E-03
```

```
32500, 5.59E-03
*SOLID SECTION, ELSET=PID13, MATERIAL=MID13
*MATERIAL, NAME=MID13
*ELASTIC
7.77E6,0.33
*PLASTIC
10000, 0.00E+00
15000, 1.71E-04
20000, 4.92E-04
30000, 2.91E-03
32500, 4.20E-03
*SOLID SECTION, ELSET=PID14, MATERIAL=MID14
*MATERIAL, NAME=MID14
*ELASTIC
8.05E6,0.33
*PLASTIC
10000, 0.00E+00
15000, 1.15E-04
20000, 3.29E-04
30000, 1.95E-03
32500, 2.81E-03
*SOLID SECTION, ELSET=PID15, MATERIAL=MID15
*MATERIAL, NAME=MID15
*ELASTIC
8.33E6,0.33
*PLASTIC
10000, 0.00E+00
15000, 5.79E-05
20000, 1.67E-04
30000, 9.86E-04
32500, 1.42E-03
*SOLID SECTION, ELSET=PID20, MATERIAL=MID20
*MATERIAL, NAME=MID20
*ELASTIC
8.29E6,0.33
*PLASTIC
10000, 0.00E+00
15000, 2.27E-04
20000, 7.40E-04
30000, 4.66E-03
32500, 7.11E-03
*SOLID SECTION, ELSET=PID21, MATERIAL=MID21
*MATERIAL, NAME=MID21
```

```
*ELASTIC
8.36E6,0.33
*PLASTIC
10000, 0.00E+00
15000, 1.90E-04
20000, 6.17E-04
30000, 3.88E-03
32500, 5.93E-03
*SOLID SECTION, ELSET=PID22, MATERIAL=MID22
*MATERIAL, NAME=MID22
*ELASTIC
8.39E6,0.33
*PLASTIC
10000, 0.00E+00
15000, 1.52E-04
20000, 4.94E-04
30000, 3.11E-03
32500, 4.75E-03
*SOLID SECTION, ELSET=PID23, MATERIAL=MID23
*MATERIAL, NAME=MID23
*ELASTIC
8.43E6,0.33
*PLASTIC
10000, 0.00E+00
15000, 1.14E-04
20000, 3.71E-04
30000, 2.34E-03
32500, 3.57E-03
*SOLID SECTION, ELSET=PID24, MATERIAL=MID24
*MATERIAL, NAME=MID24
*ELASTIC
8.46E6,0.33
*PLASTIC
10000, 0.00E+00
15000, 7.64E-05
20000, 2.49E-04
30000, 1.56E-03
32500, 2.39E-03
*SOLID SECTION, ELSET=PID25, MATERIAL=MID25
*MATERIAL, NAME=MID25
*ELASTIC
8.50E6,0.33
*PLASTIC
```

```
10000, 0.00E+00
15000, 3.86E-05
20000, 1.26E-04
30000, 7.92E-04
32500, 1.21E-03
*SOLID SECTION, ELSET=PID30, MATERIAL=MID30
*MATERIAL, NAME=MID30
*ELASTIC
9.91E6,0.33
*PLASTIC
10000, 0.00E+00
15000, 1.14E-04
20000, 5.00E-04
30000, 3.51E-03
32500, 5.84E-03
*SOLID SECTION, ELSET=PID31, MATERIAL=MID31
*MATERIAL, NAME=MID31
*ELASTIC
9.50E6,0.33
*PLASTIC
10000, 0.00E+00
15000, 9.49E-05
20000, 4.17E-04
30000, 2.93E-03
32500, 4.87E-03
*SOLID SECTION, ELSET=PID32, MATERIAL=MID32
*MATERIAL, NAME=MID32
*ELASTIC
9.29E6,0.33
*PLASTIC
10000, 0.00E+00
15000, 7.60E-05
20000, 3.34E-04
30000, 2.35E-03
32500, 3.90E-03
*SOLID SECTION, ELSET=PID33, MATERIAL=MID33
*MATERIAL, NAME=MID33
*ELASTIC
9.08E6,0.33
*PLASTIC
10000, 0.00E+00
15000, 5.71E-05
20000, 2.51E-04
```

```
30000, 1.76E-03
32500, 2.93E-03
*SOLID SECTION, ELSET=PID34, MATERIAL=MID34
*MATERIAL, NAME=MID34
*ELASTIC
8.87E6,0.33
*PLASTIC
10000, 0.00E+00
15000, 3.82E-05
20000, 1.68E-04
30000, 1.18E-03
32500, 1.96E-03
*SOLID SECTION, ELSET=PID35, MATERIAL=MID35
*MATERIAL, NAME=MID35
*ELASTIC
8.66E6,0.33
*PLASTIC
10000, 0.00E+00
15000, 1.93E-05
20000, 8.49E-05
30000, 5.97E-04
32500, 9.93E-04
*SOLID SECTION, ELSET=PID40, MATERIAL=MID40
*MATERIAL, NAME=MID40
*ELASTIC
11.5E6,0.33
*PLASTIC
15000, 0.00E+00
20000, 2.59E-04
22500, 3.89E-04
25000, 7.18E-04
27500, 1.34E-03
30000, 2.37E-03
32500, 4.57E-03
*SOLID SECTION, ELSET=PID41, MATERIAL=MID41
*MATERIAL, NAME=MID41
*ELASTIC
10.6E6,0.33
*PLASTIC
15000, 0.00E+00
20000, 2.16E-04
22500, 3.25E-04
25000, 5.99E-04
```

```
27500, 1.12E-03
30000, 1.97E-03
32500, 3.81E-03
*SOLID SECTION, ELSET=PID42, MATERIAL=MID42
*MATERIAL, NAME=MID42
*ELASTIC
10.2E6,0.33
*PLASTIC
15000, 0.00E+00
20000, 1.73E-04
22500, 2.60E-04
25000, 4.80E-04
27500, 8.98E-04
30000, 1.58E-03
32500, 3.05E-03
*SOLID SECTION, ELSET=PID43, MATERIAL=MID43
*MATERIAL, NAME=MID43
*ELASTIC
9.74E6,0.33
*PLASTIC
15000, 0.00E+00
20000, 1.30E-04
22500, 1.95E-04
25000, 3.61E-04
27500, 6.75E-04
30000, 1.19E-03
32500, 2.30E-03
*SOLID SECTION, ELSET=PID44, MATERIAL=MID44
*MATERIAL, NAME=MID44
*ELASTIC
9.29E6,0.33
*PLASTIC
15000, 0.00E+00
20000, 8.69E-05
22500, 1.31E-04
25000, 2.41E-04
27500, 4.52E-04
30000, 7.95E-04
32500, 1.54E-03
*SOLID SECTION, ELSET=PID45, MATERIAL=MID45
*MATERIAL, NAME=MID45
*ELASTIC
8.82E6,0.33
```

```
*PLASTIC
15000, 0.00E+00
20000, 4.40E-05
22500, 6.62E-05
25000, 1.22E-04
27500, 2.29E-04
30000, 4.02E-04
32500, 7.77E-04
*SOLID SECTION, ELSET=PID60, MATERIAL=MID60
*MATERIAL, NAME=MID60
*ELASTIC
11.3E6,0.33
*PLASTIC
15000, 0.00E+00
20000, 2.15E-04
22500, 3.24E-04
25000, 6.31E-04
27500, 1.10E-03
30000, 1.97E-03
32500, 3.73E-03
*SOLID SECTION, ELSET=PID61, MATERIAL=MID61
*MATERIAL, NAME=MID61
*ELASTIC
10.7E6,0.33
*PLASTIC
15000, 0.00E+00
20000, 1.79E-04
22500, 2.70E-04
25000, 5.26E-04
27500, 9.20E-04
30000, 1.64E-03
32500, 3.11E-03
*SOLID SECTION, ELSET=PID62, MATERIAL=MID62
*MATERIAL, NAME=MID62
*ELASTIC
10.4E6,0.33
*PLASTIC
15000, 0.00E+00
20000, 1.44E-04
22500, 2.16E-04
25000, 4.22E-04
27500, 7.37E-04
30000, 1.32E-03
```

```
32500, 2.49E-03
*SOLID SECTION, ELSET=PID63, MATERIAL=MID63
*MATERIAL, NAME=MID63
*ELASTIC
10.1E6,0.33
*PLASTIC
15000, 0.00E+00
20000, 1.08E-04
22500, 1.63E-04
25000, 3.17E-04
27500, 5.54E-04
30000, 9.90E-04
32500, 1.87E-03
*SOLID SECTION, ELSET=PID64, MATERIAL=MID64
*MATERIAL, NAME=MID64
*ELASTIC
9.76E6,0.33
*PLASTIC
15000, 0.00E+00
20000, 7.22E-05
22500, 1.09E-04
25000, 2.12E-04
27500, 3.71E-04
30000, 6.62E-04
32500, 1.25E-03
*SOLID SECTION, ELSET=PID65, MATERIAL=MID65
*MATERIAL, NAME=MID65
*ELASTIC
9.45E6,0.33
*PLASTIC
15000, 0.00E+00
20000, 3.66E-05
22500, 5.50E-05
25000, 1.07E-04
27500, 1.88E-04
30000, 3.35E-04
32500, 6.34E-04
*SOLID SECTION, ELSET=PID70, MATERIAL=MID70
*MATERIAL, NAME=MID70
*ELASTIC
11.0E6,0.33
*PLASTIC
15000, 0.00E+00
```

```
20000, 1.71E-04
22500, 2.58E-04
25000, 5.44E-04
27500, 8.62E-04
30000, 1.58E-03
32500, 2.88E-03
*SOLID SECTION, ELSET=PID71, MATERIAL=MID71
*MATERIAL, NAME=MID71
*ELASTIC
10.7E6,0.33
*PLASTIC
15000, 0.00E+00
20000, 1.43E-04
22500, 2.15E-04
25000, 4.54E-04
27500, 7.19E-04
30000, 1.32E-03
32500, 2.41E-03
*SOLID SECTION, ELSET=PID72, MATERIAL=MID72
*MATERIAL, NAME=MID72
*ELASTIC
10.5E6,0.33
*PLASTIC
15000, 0.00E+00
20000, 1.14E-04
22500, 1.73E-04
25000, 3.63E-04
27500, 5.76E-04
30000, 1.05E-03
32500, 1.93E-03
*SOLID SECTION, ELSET=PID73, MATERIAL=MID73
*MATERIAL, NAME=MID73
*ELASTIC
10.4E6,0.33
*PLASTIC
15000, 0.00E+00
20000, 8.60E-05
22500, 1.30E-04
25000, 2.73E-04
27500, 4.33E-04
30000, 7.92E-04
32500, 1.45E-03
*SOLID SECTION, ELSET=PID74, MATERIAL=MID74
```

```
*MATERIAL, NAME=MID74
*ELASTIC
10.2E6,0.33
*PLASTIC
15000, 0.00E+00
20000, 5.76E-05
22500, 8.68E-05
25000, 1.83E-04
27500, 2.90E-04
30000, 5.30E-04
32500, 9.69E-04
*SOLID SECTION, ELSET=PID75, MATERIAL=MID75
*MATERIAL, NAME=MID75
*ELASTIC
10.1E6,0.33
*PLASTIC
15000, 0.00E+00
20000, 2.91E-05
22500, 4.39E-05
25000, 9.24E-05
27500, 1.47E-04
30000, 2.68E-04
32500, 4.90E-04
*SOLID SECTION, ELSET=PID80, MATERIAL=MID80
*MATERIAL, NAME=MID80
*ELASTIC
10.7E6,0.33
*PLASTIC
15000, 0.00E+00
20000, 1.28E-04
22500, 1.93E-04
25000, 4.56E-04
27500, 6.20E-04
30000, 1.18E-03
32500, 2.04E-03
*SOLID SECTION, ELSET=PID81, MATERIAL=MID81
*MATERIAL, NAME=MID81
*ELASTIC
10.7E6,0.33
*PLASTIC
15000, 0.00E+00
20000, 1.06E-04
22500, 1.61E-04
```

```
25000, 3.80E-04
27500, 5.17E-04
30000, 9.85E-04
32500, 1.70E-03
*SOLID SECTION, ELSET=PID82, MATERIAL=MID82
*MATERIAL, NAME=MID82
*ELASTIC
10.7E6,0.33
*PLASTIC
15000, 0.00E+00
20000, 8.52E-05
22500, 1.29E-04
25000, 3.05E-04
27500, 4.14E-04
30000, 7.89E-04
32500, 1.36E-03
*SOLID SECTION, ELSET=PID83, MATERIAL=MID83
*MATERIAL, NAME=MID83
*ELASTIC
10.8E6,0.33
*PLASTIC
15000, 0.00E+00
20000, 6.41E-05
22500, 9.66E-05
25000, 2.29E-04
27500, 3.11E-04
30000, 5.93E-04
32500, 1.02E-03
*SOLID SECTION, ELSET=PID84, MATERIAL=MID84
*MATERIAL, NAME=MID84
*ELASTIC
10.7E6,0.33
*PLASTIC
15000, 0.00E+00
20000, 4.29E-05
22500, 6.47E-05
25000, 1.53E-04
27500, 2.08E-04
30000, 3.97E-04
32500, 6.85E-04
*SOLID SECTION, ELSET=PID85, MATERIAL=MID85
*MATERIAL, NAME=MID85
*ELASTIC
```

```
10.7E6,0.33
*PLASTIC
15000, 0.00E+00
20000, 2.17E-05
22500, 3.27E-05
25000, 7.76E-05
27500, 1.05E-04
30000, 2.01E-04
32500, 3.47E-04
*SOLID SECTION, ELSET=PID100, MATERIAL=MID100
*MATERIAL, NAME=MID100
*ELASTIC
10.8E6,0.33
*PLASTIC
15000, 0.00E+00
20000, 1.06E-04
22500, 2.09E-04
25000, 4.46E-04
27500, 6.15E-04
30000, 1.15E-03
32500, 2.01E-03
*SOLID SECTION, ELSET=PID101, MATERIAL=MID101
*MATERIAL, NAME=MID101
*ELASTIC
10.8E6,0.33
*PLASTIC
15000, 0.00E+00
20000, 8.82E-05
22500, 1.75E-04
25000, 3.72E-04
27500, 5.13E-04
30000, 9.58E-04
32500, 1.68E-03
*SOLID SECTION, ELSET=PID102, MATERIAL=MID102
*MATERIAL, NAME=MID102
*ELASTIC
10.8E6,0.33
*PLASTIC
15000, 0.00E+00
20000, 7.06E-05
22500, 1.40E-04
25000, 2.98E-04
27500, 4.11E-04
```

```
30000, 7.67E-04
32500, 1.34E-03
*SOLID SECTION, ELSET=PID103, MATERIAL=MID103
*MATERIAL, NAME=MID103
*ELASTIC
10.8E6,0.33
*PLASTIC
15000, 0.00E+00
20000, 5.31E-05
22500, 1.05E-04
25000, 2.24E-04
27500, 3.09E-04
30000, 5.77E-04
32500, 1.01E-03
*SOLID SECTION, ELSET=PID104, MATERIAL=MID104
*MATERIAL, NAME=MID104
*ELASTIC
10.8E6,0.33
*PLASTIC
15000, 0.00E+00
20000, 3.55E-05
22500, 7.04E-05
25000, 1.50E-04
27500, 2.07E-04
30000, 3.86E-04
32500, 6.76E-04
*SOLID SECTION, ELSET=PID105, MATERIAL=MID105
*MATERIAL, NAME=MID105
*ELASTIC
10.8E6,0.33
*PLASTIC
15000, 0.00E+00
20000, 1.80E-05
22500, 3.56E-05
25000, 7.58E-05
27500, 1.05E-04
30000, 1.95E-04
32500, 3.42E-04
*SOLID SECTION, ELSET=PID110, MATERIAL=MID110
*MATERIAL, NAME=MID110
*ELASTIC
10.8E6,0.33
*PLASTIC
```

15000, 0.00E+00
20000, 8.39E-05
22500, 2.26E-04
25000, 4.35E-04
27500, 6.10E-04
30000, 1.12E-03
32500, 1.99E-03
*SOLID SECTION, ELSET=PID111, MATERIAL=MID111
*MATERIAL, NAME=MID111
*ELASTIC
10.8E6,0.33
*PLASTIC
15000, 0.00E+00
20000, 6.99E-05
22500, 1.89E-04
25000, 3.63E-04
27500, 5.09E-04
30000, 9.31E-04
32500, 1.66E-03
*SOLID SECTION, ELSET=PID112, MATERIAL=MID112
*MATERIAL, NAME=MID112
*ELASTIC
10.8E6,0.33
*PLASTIC
15000, 0.00E+00
20000, 5.60E-05
22500, 1.51E-04
25000, 2.91E-04
27500, 4.08E-04
30000, 7.46E-04
32500, 1.33E-03
*SOLID SECTION, ELSET=PID113, MATERIAL=MID113
*MATERIAL, NAME=MID113
*ELASTIC
10.8E6,0.33
*PLASTIC
15000, 0.00E+00
20000, 4.21E-05
22500, 1.14E-04
25000, 2.18E-04
27500, 3.06E-04
30000, 5.60E-04
32500, 9.96E-04

20000, 3.11E-05

```
*SOLID SECTION, ELSET=PID114, MATERIAL=MID114
*MATERIAL, NAME=MID114
*ELASTIC
10.8E6,0.33
*PLASTIC
15000, 0.00E+00
20000, 2.82E-05
22500, 7.60E-05
25000, 1.46E-04
27500, 2.05E-04
30000, 3.75E-04
32500, 6.67E-04
*SOLID SECTION, ELSET=PID115, MATERIAL=MID115
*MATERIAL, NAME=MID115
*ELASTIC
10.8E6,0.33
*PLASTIC
15000, 0.00E+00
20000, 1.43E-05
22500, 3.85E-05
```

```
*ELASTIC
10.8E6,0.33
*PLASTIC
15000, 0.00E+00
20000, 1.05E-05
22500, 4.14E-05
25000, 7.21E-05
27500, 1.03E-04
30000, 1.84E-04
32500, 3.33E-04
*SOLID SECTION, ELSET=PID140, MATERIAL=MID140
*MATERIAL, NAME=MID140
*ELASTIC
12.9E6,0.33
*PLASTIC
10000, 0.00E+00
15000, 1.28E-05
20000, 4.13E-05
```

```
30000, 1.27E-04
32500, 2.40E-04
```

```
10000, 0.00E+00
15000, 1.29E-05
22500, 4.08E-05
25000, 7.11E-05
27500, 1.13E-04
30000, 2.06E-04
32500, 4.33E-04
*SOLID SECTION, ELSET=PID154, MATERIAL=MID154
*MATERIAL, NAME=MID154
*ELASTIC
12.2E6,0.33
*PLASTIC
10000, 0.00E+00
15000, 8.62E-06
22500, 2.73E-05
25000, 4.76E-05
27500, 7.58E-05
30000, 1.38E-04
32500, 2.90E-04
*SOLID SECTION, ELSET=PID155, MATERIAL=MID155
*MATERIAL, NAME=MID155
*ELASTIC
11.7E6,0.33
*PLASTIC
10000, 0.00E+00
15000, 4.36E-06
22500, 1.38E-05
25000, 2.41E-05
27500, 3.83E-05
30000, 6.99E-05
32500, 1.47E-04
*SOLID SECTION, ELSET=PID160, MATERIAL=MID160
*MATERIAL, NAME=MID160
*ELASTIC
15.6E6,0.33
*PLASTIC
25000, 0.00E+00
27500, 3.52E-05
30000, 7.42E-05
32500, 3.12E-04
*SOLID SECTION, ELSET=PID161, MATERIAL=MID161
*MATERIAL, NAME=MID161
*ELASTIC
```

```
14.6E6,0.33
*PLASTIC
25000, 0.00E+00
27500, 2.94E-05
30000, 6.19E-05
32500, 2.60E-04
*SOLID SECTION, ELSET=PID162, MATERIAL=MID162
*MATERIAL, NAME=MID162
*ELASTIC
14.1E6,0.33
*PLASTIC
25000, 0.00E+00
27500, 2.35E-05
30000, 4.95E-05
32500, 2.09E-04
*SOLID SECTION, ELSET=PID163, MATERIAL=MID163
*MATERIAL, NAME=MID163
*ELASTIC
13.6E6,0.33
*PLASTIC
25000, 0.00E+00
27500, 1.77E-05
30000, 3.72E-05
32500, 1.57E-04
*SOLID SECTION, ELSET=PID164, MATERIAL=MID164
*MATERIAL, NAME=MID164
*ELASTIC
13.0E6,0.33
*PLASTIC
25000, 0.00E+00
27500, 1.18E-05
30000, 2.49E-05
32500, 1.05E-04
*SOLID SECTION, ELSET=PID165, MATERIAL=MID165
*MATERIAL, NAME=MID165
*ELASTIC
12.5E6,0.33
*PLASTIC
25000, 0.00E+00
27500, 5.99E-06
30000, 1.26E-05
32500, 5.31E-05
**  LOAD CASE   100
```

```
*PREPRINT,ECHO=NO,HISTORY=NO,MODEL=YES
**
*STEP,INC=20
LOAD CASE   100
*STATIC,DIRECT
0.5000E-01 1.000
*** Load-100
**
*DLOAD, OP=NEW
   4105, P4,    -32500.
   4114, P4,    -32500.
   4123, P4,    -32500.
   4132, P4,    -32500.
   4141, P4,    -32500.
   4150, P4,    -32500.
   4159, P4,    -32500.
   4168, P4,    -32500.
   4177, P4,    -32500.
   4186, P4,    -32500.
   4195, P4,    -32500.
   4204, P4,    -32500.
   4213, P4,    -32500.
   4222, P4,    -32500.
   4231, P4,    -32500.
   4240, P4,    -32500.
   4249, P4,    -32500.
   4258, P4,    -32500.
   4267, P4,    -32500.
   4276, P4,    -32500.
   4285, P4,    -32500.
   4294, P4,    -32500.
   4303, P4,    -32500.
   4312, P4,    -32500.
   4321, P4,    -32500.
   4330, P4,    -32500.
   4339, P4,    -32500.
   4348, P4,    -32500.
   4357, P4,    -32500.
   4366, P4,    -32500.
   4375, P4,    -32500.
   4384, P4,    -32500.
   4393, P4,    -32500.
   4402, P4,    -32500.
```

```
   4411, P4,    -32500.
   4420, P4,    -32500.
   4429, P4,    -32500.
   4438, P4,    -32500.
   4447, P4,    -32500.
   4456, P4,    -32500.
   4465, P4,    -32500.
   4474, P4,    -32500.
   4483, P4,    -32500.
   4492, P4,    -32500.
   4501, P4,    -32500.
   4510, P4,    -32500.
   4519, P4,    -32500.
   4528, P4,    -32500.
   4537, P4,    -32500.
   4546, P4,    -32500.
   4555, P4,    -32500.
   4564, P4,    -32500.
   4573, P4,    -32500.
   4582, P4,    -32500.
   4591, P4,    -32500.
   4600, P4,    -32500.
   4609, P4,    -32500.
   4618, P4,    -32500.
   4627, P4,    -32500.
   4636, P4,    -32500.
   4645, P4,    -32500.
   4654, P4,    -32500.
   4663, P4,    -32500.
   4672, P4,    -32500.
**
*FILE FORMAT ASCII
*EL PRINT,FREQ=0
*NODE PRINT,FREQ=0
*NODE FILE, GLOBAL=YES,FREQ=20
U
*EL FILE,POSITION=CENTROIDAL,FREQ=1
S
E
PE
*END STEP
```

APPENDIX C

COMPARISON OF ANALYTICAL RESULTS TO *ABAQUS* RESULTS

Comparison of Analytical and Computational Methods

$$\varepsilon_x = \frac{\left(\frac{\sqrt{2}}{3a}\sigma_e\right)^{\frac{1}{b}}}{\sqrt{2}\sigma_e}\left[\sigma_x - \frac{1}{2}(\sigma_y + \sigma_z)\right] \qquad \varepsilon_z = \frac{\left(\frac{\sqrt{2}}{3a}\sigma_e\right)^{\frac{1}{b}}}{\sqrt{2}\sigma_e}\left[\sigma_z - \frac{1}{2}(\sigma_x + \sigma_y)\right]$$

$$\varepsilon_y = \frac{\left(\frac{\sqrt{2}}{3a}\sigma_e\right)^{\frac{1}{b}}}{\sqrt{2}\sigma_e}\left[\sigma_y - \frac{1}{2}(\sigma_x + \sigma_z)\right]$$

Weld Material Constants

a	*b*
4.72E+04	0.237

Analytical Equations				***ABAQUS Results (Converted to Eng. Strains)***			
Strain x	***Strain y***	***Strain z***	$\varepsilon_x^p + \varepsilon_y^p + \varepsilon_z^p = 0$	***Strain x***	***Strain y***	***Strain z***	$\varepsilon_x^p + \varepsilon_y^p + \varepsilon_z^p = 0$
0.00E+00	0.00E+00	0.00E+00	0.0000	0.00E+00	0.00E+00	0.00E+00	0.0000
3.63E-08	-1.82E-08	-1.82E-08	0.0000	0.00E+00	0.00E+00	0.00E+00	0.0000
6.77E-07	-3.38E-07	-3.38E-07	0.0000	0.00E+00	0.00E+00	0.00E+00	0.0000
3.74E-06	-1.87E-06	-1.87E-06	0.0000	0.00E+00	0.00E+00	0.00E+00	0.0000
1.26E-05	-6.30E-06	-6.30E-06	0.0000	0.00E+00	0.00E+00	0.00E+00	0.0000
3.23E-05	-1.62E-05	-1.62E-05	0.0000	0.00E+00	0.00E+00	0.00E+00	0.0000
6.97E-05	-3.49E-05	-3.49E-05	0.0000	1.30E-04	-6.51E-05	-6.51E-05	0.0000
1.34E-04	-6.68E-05	-6.68E-05	0.0000	2.89E-04	-1.44E-04	-1.44E-04	0.0000
2.34E-04	-1.17E-04	-1.17E-04	0.0000	4.47E-04	-2.24E-04	-2.24E-04	0.0000
3.85E-04	-1.93E-04	-1.93E-04	0.0000	6.06E-04	-3.03E-04	-3.03E-04	0.0000
6.00E-04	-3.00E-04	-3.00E-04	0.0000	7.65E-04	-3.82E-04	-3.82E-04	0.0000
8.96E-04	-4.48E-04	-4.48E-04	0.0000	9.30E-04	-4.65E-04	-4.65E-04	0.0000
1.29E-03	-6.46E-04	-6.46E-04	0.0000	1.29E-03	-6.43E-04	-6.43E-04	0.0000
1.81E-03	-9.03E-04	-9.03E-04	0.0000	1.88E-03	-9.38E-04	-9.38E-04	0.0000
2.46E-03	-1.23E-03	-1.23E-03	0.0000	2.57E-03	-1.28E-03	-1.28E-03	0.0000
3.28E-03	-1.64E-03	-1.64E-03	0.0000	3.48E-03	-1.74E-03	-1.74E-03	0.0000
4.29E-03	-2.15E-03	-2.14E-03	0.0000	4.52E-03	-2.25E-03	-2.25E-03	0.0000
5.51E-03	-2.76E-03	-2.75E-03	0.0000	5.75E-03	-2.87E-03	-2.86E-03	0.0000
6.98E-03	-3.49E-03	-3.49E-03	0.0000	6.98E-03	-3.48E-03	-3.47E-03	0.0000
8.70E-03	-4.35E-03	-4.35E-03	0.0000	8.63E-03	-4.29E-03	-4.29E-03	0.0001
1.07E-02	-5.35E-03	-5.34E-03	0.0000	1.09E-02	-5.42E-03	-5.41E-03	0.0001

REPORT DOCUMENTATION PAGE

Form Approved
OMB No. 0704-0188

1. AGENCY USE ONLY (Leave blank)	2. REPORT DATE	3. REPORT TYPE AND DATES COVERED
	September 1994	Technical Paper

4. TITLE AND SUBTITLE
An Inelastic Analysis of a Welded Aluminum Joint

5. FUNDING NUMBERS

6. AUTHOR(S)
R.E. Vaughan

7. PERFORMING ORGANIZATION NAME(S) AND ADDRESS(ES)
George C. Marshall Space Flight Center
Marshall Space Flight Center, Alabama 35812

8. PERFORMING ORGANIZATION REPORT NUMBER
M-760

9. SPONSORING/MONITORING AGENCY NAME(S) AND ADDRESS(ES)
National Aeronautics and Space Administration
Washington, DC 20546

10. SPONSORING/MONITORING AGENCY REPORT NUMBER
NASA TP-3508

11. SUPPLEMENTARY NOTES
Prepared by Structures and Dynamics Laboratory, Science and Engineering Directorate.

12a. DISTRIBUTION/AVAILABILITY STATEMENT
Subject Category: 39
Unclassified—Unlimited

12b. DISTRIBUTION CODE

13. ABSTRACT *(Maximum 200 words)*

Butt-weld joints are most commonly designed into pressure vessels which then become as reliable as the weakest increment in the weld chain. In practice, weld material properties are determined from tensile test specimen and provided to the stress analyst in the form of a stress versus strain diagram. Variations in properties through the thickness of the weld and along the width of the weld have been suspect but not explored because of inaccessibility and cost.

The purpose of this study is to investigate analytical and computational methods used for analysis of welds. The weld specimens are analyzed using classical elastic and plastic theory to provide a basis for modeling the inelastic properties in a finite-element solution. The results of the analysis are compared to experimental data to determine the weld behavior and the accuracy of prediction methods. The weld considered in this study is a multiple-pass aluminum 2219-T87 butt weld with thickness of 1.40 in.

The weld specimen is modeled using the finite-element code *ABAQUS*. The finite-element model is used to produce the stress-strain behavior in the elastic and plastic regimes and to determine Poisson's ratio in the plastic region. The value of Poisson's ratio in the plastic regime is then compared to experimental data. The results of the comparisons are used to explain multipass weld behavior and to make recommendations concerning the analysis and testing of welds.

14. SUBJECT TERMS	15. NUMBER OF PAGES
plastic analysis, nonlinear analysis, incremental strain theory, multipass welds, thick welds	81
	16. PRICE CODE: A05

17. SECURITY CLASSIFICATION OF REPORT	18. SECURITY CLASSIFICATION OF THIS PAGE	19. SECURITY CLASSIFICATION OF ABSTRACT	20. LIMITATION OF ABSTRACT
Unclassified	Unclassified	Unclassified	Unlimited